JOURNAL OF PROPULSION AND POWER
Vol. 33, No. 3, May–June 2017

Rate-Controlled Constrained Equilibrium for Nozzle and Shock Flows

Jason Rabinovitch* and Guillaume Blanquart†
California Institute of Technology, Pasadena, California 91125

DOI: 10.2514/1.B36226

The performance of different constraints for the rate-controlled constrained-equilibrium (RCCE) method is investigated in the context of modeling reacting flows characteristic of hypervelocity ground testing facilities and reentry conditions. Although the RCCE approach has been used widely in the past, its application in non-combustion-based reacting flows is rarely done; the flows being investigated in this work do not contain species that can easily be classified as reactants and/or products. The effectiveness of different constraints is investigated before running a full computational simulation, and new constraints not reported in the existing literature are introduced. A constraint based on the enthalpy of formation is shown to work well for the two gas models used for flows that involve both shocks and steady expansions.

Nomenclature

C	=	constraint coefficient
c_P	=	specific heat at constant pressure, J/(kg · K)
d	=	nozzle diameter, m
e	=	specific internal energy, J/kg
$\boldsymbol{e}$	=	right eigenvector of Jacobian matrix, s^{-1}
h	=	specific enthalpy, J/kg
Δh_f°	=	enthalpy of formation, kJ/mol
$h_i(T_o)$	=	reference enthalpy of a mixture, J/kg
$\boldsymbol{J}$	=	time-dependent Jacobian matrix, s^{-1}
ne	=	number of elements
ns	=	number of species
P	=	pressure, Pa
$\mathcal{R}$	=	universal gas constant, 8.314 J/(mol · K)
R	=	specific gas constant, J/(kg · K)
r^+	=	forward reaction rate, mol/(m^3 · s)
r^-	=	backward reaction rate, mol/(m^3 · s)
T	=	temperature, K
t	=	time, s
t^*	=	characteristic timescale of a reaction mode, s
$\boldsymbol{u}$	=	cartesian velocity vector
u, v, w	=	velocities in the x, y, and z directions
w	=	velocity in the x direction in the shock-fixed frame
W	=	molecular weight, kg/mol
$\overline{W}$	=	mixture averaged molecular weight, kg/mol
X	=	mole fraction
x	=	location downstream of the shock or nozzle throat, m
Y	=	mass fraction
η	=	sonic parameter
γ	=	ratio of specific heats for a mixture
λ	=	eigenvalue of Jacobian matrix, s^{-1}
$\boldsymbol{\nu}^*$	=	eigenvector associated with the fastest reaction mode, s^{-1}
$\overline{\boldsymbol{\nu}^*}$	=	average reaction mode vector, s^{-1}
$\dot{\omega}$	=	net production rate, mol/(m^3 · s)
Ω	=	chemical source term, s^{-1}
ϕ	=	rate-controlled constrained-equilibrium constraint variable
ρ	=	mass density, kg/m^3
$\dot{\sigma}$	=	thermicity, s^{-1}

Subscripts

i	=	species index
l	=	spatial location

Superscripts

CEQ	=	constrained thermodynamic equilibrium values
k	=	chosen constraint
R	=	properties calculated from the fully integrated rate-controlled constrained-equilibrium simulation
RCEQ	=	reconstructed value

Received 25 February 2016; revision received 21 August 2016; accepted for publication 22 August 2016; published online 14 November 2016.

*Postdoctoral Scholar, Mechanical Engineering, 1200 East California Boulevard, MC 205-45. Now Mechanical Engineer, Jet Propulsion Laboratory, California Institute of Technology, Pasadena, CA, M/S T1708. Member AIAA.

†Professor, Mechanical Engineering, 1200 East California Boulevard, MC 107-81. Member AIAA.

I. Introduction

AT THE high speeds reached by reentry vehicles entering an atmosphere, not only is the vehicle traveling in a hypersonic regime (Mach number $\gtrsim 5$), but also the ordered kinetic energy per unit mass of the gas (which for a body moving at U_∞ can be approximated as $U_\infty^2/2$) is of the same order of the relevant thermochemical energy scales in the flow [1]. In this regime, the velocity is so large that the conditions behind a bow shock on a reentry vehicle cause the molecular components of the gas to dissociate. The chemical composition and properties of the flow can no longer be assumed to be constant, and thermochemical effects must be accounted for. These effects must be taken into account when modeling reentry flight conditions and when used to simulate high-enthalpy flows in ground testing facilities. As these effects cannot be predicted analytically, they must be modeled numerically [1].

To accurately simulate flows that are highly compressible, viscous, chemically reacting, and possibly in thermal and chemical nonequilibrium, a computational method to handle chemical reactions must be implemented into a computational fluid dynamics (CFD) solver. There is a large increase in computational cost when moving from nonreacting to reacting flows; a transport equation and a chemical source term for each species considered must now be included (e.g., see [2]). In the past, there has been a significant amount of effort put into reducing chemical models so that a relatively large set of stiff ODEs need not be solved in conjunction with the fluid flow. Many methods are either based on reducing the chemical model used to a manageable size, or to introduce tabulated chemistry [3–9].

One class of methods that are geared toward reducing the size of a chemical model is based on separating chemical reactions by

timescales. This class of methods includes computational singular perturbation (CSP) and intrinsic lower-dimensional manifolds (ILDM) [10–12]. "Slow" reactions (associated with large timescales) are solved, whereas "fast" reactions (associated with small timescales) are put into local equilibrium. Keck [13–16] proposed a similar method, except that his method relies more on the thermodynamic properties of the species present, rather than on the chemical reaction rates. This method, referred to as rate-controlled constrained-equilibrium (RCCE), tracks one or several constraints through the system, and reconstructs the system as a function of the constraint(s), based on constrained thermodynamic equilibrium calculations. Examples of possible constraints include the mass fraction of a single major species, radical species (species with valence electrons), or any linear combination of species mass fractions. In general, only the reaction rates associated with the rate of change of the constraint variable need to be known for this method. Both the state of the system and the rate of change of the constraint can be tabulated, and then efficient methods can be used to incorporate this tabulated chemistry into a CFD solver. An overview of the RCCE method and a summary of its advantages and disadvantages have previously been performed by Keck [14].

The RCCE method has been applied successfully to laminar and turbulent flames under low Mach conditions in the past [13–15,17–30]. Unfortunately, there is little available data detailing the performance of the RCCE method for compressible flows [31,32], and none of it pertains to hypervelocity conditions. Therefore, the goal of this paper is to investigate different possible constraints to be used with the RCCE method for reacting compressible flows, and to investigate the predicted performance of the constraints before running a full RCCE simulation. Specifically, this work focuses on using the RCCE method to model reacting compressible nozzle and shock flows.

The paper is organized as follows. Sections II and III summarize previous work performed with the RCCE method, and present the reacting Euler equations that are used in this work. Sections IV–VI outline how the RCCE method is used in this work and what constraints are chosen, and explain the conditions for the specific test problems considered. Specifically, the effectiveness of different constraints is isolated by performing a point-wise comparison of results based on constrained thermodynamic equilibrium calculations to detailed chemistry results. These results are shown in Sec. VIII, and are not based on integrated RCCE simulations. The results from this comparison allow an appropriate constraint to be selected for full RCCE simulations, and help one understand the limits of the applicability of the RCCE method for the test cases considered. Results from full RCCE simulations are then shown in Sec. IX. Preliminary work on this subject has been previously published by the authors [33].

II. Previous Work

The RCCE method has been used in a variety of studies in the past with large degrees of success, and these studies are summarized in this section. In Keck's work [14], a detailed description of the RCCE method is provided, as well as an overview of RCCE results obtained in other studies. In an earlier study, Keck and Gillespie [22] compared steady-state calculations with results obtained using the RCCE method for the formation and removal of NO in an internal combustion engine. Later, Morr and Heywood [34] used the RCCE method to analyze measurements of CO concentrations in a steady-flow cylindrical burner, and Yousefian [30] used the RCCE method to predict the quenching of CO in cooled combustion streams. Law et al. [15] investigated the performance of several different constraints when studying the reacting H_2/O_2 system, and Ugarte et al. [29] used RCCE to model the formaldehyde–oxygen combustion process. These studies showed good agreement between the RCCE method and detailed chemical models. More recently, the RCCE method has been used to show good agreement with full detailed mechanisms for complex hydrocarbon fuels [13,21], and the method has also been extended to allow for nonlinear constraints [16]. Studies have also focused on the reduction in computational time that the RCCE method provides related to using a detailed chemical mechanism [17,18], as well as investigating the effect of mixing on the RCCE methodology [18].

Keck's work [14] emphasized that only the rate constants for the reactions related to the rate of change of the chosen constraint are needed for this method, and that the benefits gained from using the RCCE method continue to increase as chemical systems become larger and more complex. With more complicated systems in mind, this has motivated investigations of the RCCE method in conjunction with tabulated approaches, such as in [27,28]. In addition, Hiremath et al. [19] have extended the basic RCCE method to investigate dynamic methods to change the constraint in order to minimize errors, but this was limited to investigating the effect of constraining different combinations of individual species. Hiremath and Pope [20] have also used the RCCE method in conjunction with Lagrangian particle probability density function–based computations.

Whereas the previously mentioned studies have all been geared toward subsonic combustion problems, Janbozorgi and Metghalchi [32] used a degree of disequilibrium analysis (Sec. V.B) to model a supersonic reacting H/O system expanding through a nozzle, and Beretta et al. [31] used a similar degree of disequilibrium analysis to apply the RCCE methodology to the steady supersonic expansion of the products of hydrogen and methane oxycombustion. All of the studies discussed that use the RCCE method have been geared toward combustion applications, where reactants and products can be distinguished. This work extends the use of the RCCE method to compressible reacting flows that are not combustion based, where it is challenging to define specific reactants and products.

III. Reacting Euler Equations

When reduced-order models are compared with detailed models, it is not always possible to compare the yield of individual species, as some species might exist only in the detailed model. Instead, one should compare the bulk properties of the fluid mixture, which a reduced-order model ought to reproduce. To determine which properties of the fluid are relevant in reacting supersonic flows, the reacting Euler equations should be considered. The 3D reacting Euler equations in conservative form are shown in Eqs. (1–3).

$$\frac{\partial \boldsymbol{w}}{\partial t} + \frac{\partial \boldsymbol{f}_x}{\partial x} + \frac{\partial \boldsymbol{f}_y}{\partial y} + \frac{\partial \boldsymbol{f}_z}{\partial z} = \boldsymbol{g} \tag{1}$$

where

$$\boldsymbol{w} = \begin{pmatrix} \rho \\ \rho u \\ \rho v \\ \rho w \\ e \\ \rho Y_1 \\ \vdots \\ \rho Y_{\text{ns}} \end{pmatrix}, \qquad \boldsymbol{f}_x = \begin{pmatrix} \rho u \\ \rho u^2 + P \\ \rho uv \\ \rho uw \\ u(E+P) \\ \rho u Y_1 \\ \vdots \\ \rho u Y_{\text{ns}} \end{pmatrix},$$

$$\boldsymbol{f}_y = \begin{pmatrix} \rho v \\ \rho uv \\ \rho v^2 + p \\ \rho vw \\ v(E+P) \\ \rho v Y_1 \\ \vdots \\ \rho v Y_{\text{ns}} \end{pmatrix}, \qquad \boldsymbol{f}_z = \begin{pmatrix} \rho w \\ \rho uw \\ \rho vw \\ \rho w^2 + P \\ w(E+P) \\ \rho w Y_1 \\ \vdots \\ \rho w Y_{\text{ns}} \end{pmatrix} \tag{2}$$

and

$$\boldsymbol{g} = \begin{pmatrix} 0 \\ 0 \\ 0 \\ 0 \\ 0 \\ \dot{\omega}_1(T, P, Y_1, \ldots, Y_{\text{ns}})W_1 \\ \vdots \\ \dot{\omega}_{\text{ns}}(T, P, Y_1, \ldots, Y_{\text{ns}})W_{\text{ns}} \end{pmatrix} \tag{3}$$

E is the total energy, which is given by

$$E = \rho\left(e + \frac{1}{2}|\boldsymbol{u}|^2\right) \tag{4}$$

where e is the specific internal energy; $|\boldsymbol{u}|^2 = u^2 + v^2 + w^2$; and u, v, and w are the velocities in the x, y, and z directions, respectively. The above equations require an equation of state for closure, such as the caloric equation of state, $P = P(\rho, e, Y_1, \ldots, Y_{\text{ns}})$. T, P, ρ, Y_i, ns, $\dot{\omega}_i$, and W_i are the temperature, pressure, density, mass fraction of species i, number of total species, net production rate of species i, and the molecular weight of species i, respectively. From a mathematical standpoint, the RCCE method alters the final ns equations given in Eqs. (2) and (3). This will be shown in more detail in Secs. IV and IX. To limit the scope of this paper, while still retaining the complexity of the chemical processes, steady one-dimensional, and quasi–one-dimensional ideal gas flows are considered.

Following the derivations performed in [35], in the shock-fixed frame, the one-dimensional reacting Euler equations can be re-written as

$$\frac{\mathrm{d}\rho}{\mathrm{d}x} = -\frac{\rho}{\mathrm{w}}\frac{\dot{\sigma}}{\eta} \tag{5}$$

$$\frac{\mathrm{dw}}{\mathrm{d}x} = \frac{\dot{\sigma}}{\eta} \tag{6}$$

$$\frac{\mathrm{d}P}{\mathrm{d}x} = -\rho\mathrm{w}\frac{\dot{\sigma}}{\eta} \tag{7}$$

$$\frac{\mathrm{d}Y_i}{\mathrm{d}x} = \dot{\omega}_i(T, P, Y_1, \ldots, Y_{\text{ns}})\frac{W_i}{\rho}\frac{1}{\mathrm{w}} \tag{8}$$

where w, $\dot{\sigma}$, and η are the velocity in the x direction in the shock-fixed frame, the thermicity, and the sonic parameter ($\eta = 1 - M^2$), respectively. Equations (5–8) can be generalized to include an area change if desired, as shown by Kao and Shepherd [35]. This extension is used to simulate nozzle flows in this work. To simplify notation, a chemical source term, Ω, is introduced such that $\Omega_i = \dot{\omega}_i(W_i/\rho)$. The thermicity is defined to be

$$\dot{\sigma} = \sum_{i=1}^{\text{ns}} \sigma_i \Omega_i \tag{9}$$

where σ_i takes the form

$$\sigma_i = \frac{\overline{W}}{W_i} - \frac{h_i}{c_P T} \tag{10}$$

assuming an ideal gas. c_P is the specific heat at constant pressure, $\overline{W}$ is the mixture averaged molecular weight, and h_i is the enthalpy of species i. For each individual species, the specific enthalpy can be calculated by

$$h_i = h_i(T_o) + \int_{T_o}^{T} c_{p,i}(T')\,\mathrm{d}T' \tag{11}$$

where $h_i(T_o)$ is the reference enthalpy at $T_o = 298$ K [36].

Whereas the Ω_i term is sensitive to individual species concentrations, the other bulk properties, $\overline{W}$ and c_p, are dominated by species with the largest mole and mass fractions (respectively), as $\overline{W} = \sum_{i=1}^{\text{ns}} X_i \cdot W_i$ and $c_p = \sum_{i=1}^{\text{ns}} c_{p_i} \cdot Y_i$. Here X_i refers to the mole fraction of species i. Although not appearing directly in the reacting Euler equations, the mixture enthalpy, $h = \sum_{i=1}^{\text{ns}} h_i \cdot Y_i$, gives an indication as to how much energy is stored in the gas (not including contributions to internal energy from pressure and volume). As a result, the overall evolution of the flow is mainly based on the bulk properties of the mixture (such as $\overline{W}$, c_p, and h). Because of this, it is believed that errors made on minor species should have a relatively small effect on the overall evolution of the reactive Euler equations. This is the major concept behind RCCE and allows for the successful application of reduced-order models that do not necessarily predict all minor species correctly, but do well predicting bulk properties of a mixture.

IV. RCCE Overview

The RCCE method relies on the assumption that a limited number of chemical properties of a mixture (constraints) can be used to reconstruct the composition of a mixture through constrained thermodynamic equilibrium calculations. One challenge associated with successfully applying the RCCE method to a given reacting system is choosing relevant constraints. Some possible constraints originally suggested by Keck [14] include tracking individual species, major species, or radical species present in a mixture. Only the chosen constraint(s) now need be solved for throughout the system, and then the rest of the mixture can be reconstructed around this/these value(s).

Mathematically, the constraint variable ϕ is often a linear function of all of the chemical species present in a mixture:

$$\phi^k = \sum_{i=1}^{\text{ns}} C_i^k Y_i \tag{12}$$

where k corresponds to a chosen constraint, and C_i^k is the coefficient associated with the ith species, for the kth constraint. To clarify notation, the superscript k is dropped for the rest of this section, and the following analysis is performed for a single ϕ. It should be understood that the C_i coefficients (constraint coefficients) will change if a different constraint is chosen. For example, if one were to constrain only the jth species in a mixture, then $C_j = 1$, and $C_{i\neq j} = 0$. The constraint is generally chosen a priori for a given simulation, and the same constraint is used throughout the entire simulation; that is, the C_i's are constant. Nonlinear constraints are not considered for this work, though have been used in other studies [16].

The superscript CEQ will be used from this point on in order to distinguish between values calculated through the use of constrained thermodynamic equilibrium calculations (CEQ superscript), and values calculated through detailed chemistry calculations (no superscript).

Values for $\boldsymbol{Y}^{\text{CEQ}}$ ($\boldsymbol{Y}^{\text{CEQ}} = [Y_1^{\text{CEQ}} \ldots Y_{\text{ns}}^{\text{CEQ}}]^T$) are calculated such that $\boldsymbol{Y}^{\text{CEQ}}$ minimizes Gibbs function, G, while keeping T, P, and ϕ constant for a specific mixture. This implies that

$$Y_i^{\text{CEQ}} = Y_i^{\text{CEQ}}(T, P, \phi) \tag{13}$$

All constrained equilibrium calculations performed to evaluate Eq. (13) are performed using the CEQ code developed by Prof. Stephen B. Pope at Cornell University [37–39]. Equation (13) implies that $\phi = \phi^{\text{CEQ}}$, by definition, where $\phi^{\text{CEQ}} = \sum_{i=1}^{\text{ns}} C_i Y_i^{\text{CEQ}}$. However, Eqs. (15) and (16) will show that the partial derivatives $\partial\phi/\partial t$ and $(\partial\phi^{\text{CEQ}}/\partial t)$ are not necessarily equal.

A chemical source term based on $\boldsymbol{Y}^{\mathrm{CEQ}}$ can now be calculated:

$$\Omega_i^{\mathrm{CEQ}} = \Omega_i(T, P, \boldsymbol{Y}^{\mathrm{CEQ}}) = \Omega_i^{\mathrm{CEQ}}(T, P, \phi) \tag{14}$$

This is in contrast to the chemical source term described previously, $\Omega_i = \Omega_i(T, P, \boldsymbol{Y})$. The difference between Ω_i^{CEQ} and Ω_i is caused by the differences between $\boldsymbol{Y}^{\mathrm{CEQ}}$ and $\boldsymbol{Y}$; the same T and P are used in both calculations.

The rate of change of the constraint must also be calculated, and this is done by differentiating Eq. (12) with respect to time:

$$\frac{\partial \phi^{\mathrm{CEQ}}}{\partial t} = \sum_{i=1}^{\mathrm{ns}} C_i \frac{\partial Y_i^{\mathrm{CEQ}}}{\partial t} = \sum_{i=1}^{\mathrm{ns}} C_i \Omega_i^{\mathrm{CEQ}} \tag{15}$$

A rate of change of the constraint can also be calculated solely based on the detailed chemistry results (for comparison purposes), and this is defined to be

$$\frac{\partial \phi}{\partial t} = \sum_{i=1}^{\mathrm{ns}} C_i \Omega_i \tag{16}$$

Finally, it is also possible to calculate bulk properties of the mixtures. For example,

$$c_p^{\mathrm{CEQ}} = \sum_{i=1}^{\mathrm{ns}} c_{p_i}(T) Y_i^{\mathrm{CEQ}} \tag{17}$$

while

$$c_p = \sum_{i=1}^{\mathrm{ns}} c_{p_i}(T) Y_i \tag{18}$$

Comparisons between the CEQ quantities and quantities calculated from detailed chemistry calculations are shown in Sec. VIII.

V. Methodology for Constraint Selection

Inherent to the RCCE method is the necessity of picking constraints to be used. This section outlines the general method for picking constraints based on time-scale analysis and a degree of disequilibrium analysis. A full explanation of all constraints considered, and how these constraints can be calculated for specific test cases will be provided later in Sec. VII.

It is important to recognize that there is no guarantee that the same constraint(s) will work for every problem investigated. The RCCE method requires some a priori intuition about the system to be investigated, or some simplified analysis to be performed. The fact that constraints must be identified before investigating a specific system can be seen as a disadvantage, yet Keck argues that this is an advantage, as it "... forces one to think before embarking on elaborate calculations!" [14].

A. Timescale Analysis

Analyzing chemical timescales has been used extensively in the past by the combustion community. The two popular methods that use timescale analysis for reduced-order modeling techniques are CSP [10] and ILDM [11,12]. These methods continue to be updated [40], but only the basic principles are needed in this section. A brief overview of CSP and ILDM is provided below for completeness.

The over-arching idea of CSP is to separate the system into "fast" and "slow" reaction subspaces, with a rigorous and repeatable mathematical method. More precisely, the reactions are divided into an "equilibrated set," which contains fast reactions that are in a local equilibrium, and a "rate-controlling" set that contains the slower reactions that control the evolution of the system. If a reaction falls into neither of these sets, then it is considered to be "superfluous." Decoupling the fastest timescales from the slowest timescales removes the stiffness from the system of ODEs, and allows the system of equations to be solved in an explicit manner with high accuracy.

Unlike CSP, which is geared toward reducing the stiffness of the system of ODEs needed to be solved, ILDM, a method first proposed by Maas and Pope [11,12], is geared toward identifying a lower-dimensional manifold that reactions are confined to. Chemical reactions can be described in terms of a state space, where the different chemical species define the different dimensions of the state space. Under the condition that h and P are constant (as assumed by Maas and Pope [12]), the reaction space is limited to a manifold of dimension ns-ne, where ns is the number of species considered, and ne is the number of elements (the subtraction of ne occurs due to elemental conservation). With this in mind, a chemical reaction can be interpreted as a trajectory in this state space. Over time, these trajectories all tend toward a point that corresponds to the thermodynamic equilibrium composition. Maas and Pope found that these reaction trajectories tend to "bunch" and approach one another long before chemical equilibrium was reached. They identified lower-dimensional manifolds that act as attractors in state space, and are governed by slow reactions. Based around the attracting manifolds in state space, the ILDM method can greatly reduce the overall order of the reacting system while still maintaining a user-defined level of accuracy.

Both the CSP and ILDM methods rely on a dynamical system approach. In general, the rate of change of mass fractions of the species present in a mixture can be written as

$$\frac{\mathrm{d}\boldsymbol{Y}}{\mathrm{d}t} = \boldsymbol{\Omega} \tag{19}$$

where $\boldsymbol{\Omega} = [\Omega_1 \Omega_2 \ldots \Omega_{\mathrm{ns}}]^T$. A small change in mass fraction is considered such that $\boldsymbol{Y} = \boldsymbol{Y}_o + \boldsymbol{Y}'$. Using a Taylor series expansion, and keeping only the linear term in $\boldsymbol{Y}'$ results in

$$\frac{\mathrm{d}\boldsymbol{Y}'}{\mathrm{d}t} = \boldsymbol{J} \cdot \boldsymbol{Y}' \tag{20}$$

where $\boldsymbol{J}$ is the time-dependent Jacobian matrix for the chemical reaction, with $J_{ij} = (\partial \Omega_i / \partial Y_j)$. If $\boldsymbol{J}$ is assumed to be constant during a small time interval (small compared with the relaxation times associated with the perturbations), the decomposition $\boldsymbol{J} = \boldsymbol{A}\Lambda\boldsymbol{B}$ can be used. $\boldsymbol{A}$ is a matrix of basis vectors, and $\boldsymbol{B} = \boldsymbol{A}^{-1}$. If $\boldsymbol{A}$ were an ideal basis matrix, then Λ would be a diagonal matrix with ns entries. However, for chemical systems in general, $\boldsymbol{J}$ is a rank-deficient, nonsymmetric, and ill-conditioned matrix. It is at most rank ns-ne.

The first ns-ne right eigenvectors (columns of $\boldsymbol{A}$), $\boldsymbol{e}_1$, $\boldsymbol{e}_1, \ldots, \boldsymbol{e}_{\text{ns-ne}}$, are reaction modes for the system. Each reaction mode is associated with a characteristic timescale, which is the inverse of the real component of the corresponding eigenvalue, λ_i. The characteristic time associated with mode i is defined to be $t_i^* = -1/Re(\lambda_i)$. A reaction mode with a small characteristic timescale relaxes to the initial state faster than a mode with a larger characteristic timescale. The eigenvector associated with the fastest reaction mode (largest eigenvalue) will be referred to as $\boldsymbol{\nu}^*$, where $\boldsymbol{\nu}^* = [\nu_1^* \ldots \nu_{\mathrm{ns}}^*]^T$. This formal timescale analysis has not been combined with RCCE previously; the reaction modes and their associated timescales will be tested as constraints, and the method used to calculate ν^* for a specific problem is presented later in Sec. VII.D.

B. Degree of Disequilibrium

Another constraint based on timescale analysis, and also one of the constraints that Keck proposed in his original work [14], is the degree of disequilibrium of an individual chemical reaction. The idea behind this constraint is to evaluate whether specific chemical reactions are in a local state of equilibrium [31,32]. This constraint, although still based on reaction timescales, is a simplified version of the timescale analysis presented in the previous section.

The degree of disequilibrium, DOD, for a specific reaction is defined to be $\mathrm{DOD} = \log(r^-/r^+)$, where r^- is the backward reaction rate, and r^+ is the forward reaction rate. When this value is close to 0,

the reaction is close to equilibrium, as $r^- \approx r^+$, and if this ratio is far from 0, then $r^- \gg r^+$ or $r^- \ll r^+$. As outlined in Sec. IV, the chosen constraint should be representative of the rate-limiting reactions that are occurring in the system. It can be reasoned that reactions that are close to equilibrium are related to relatively fast timescales, and should therefore not affect the value of the constraint (as the constraint should be affected only by reactions with slow timescales). Keeping this in mind, constraints that are independent of the fast reactions can be chosen.

A simple example is shown below for a five-species (O_2, N_2, O, N, NO) air model. It is assumed that the system can be modeled by the following five reactions:

$$O + O \rightleftarrows O_2(+M) \tag{21}$$

$$N + N \rightleftarrows N_2(+M) \tag{22}$$

$$N + O \rightleftarrows NO(+M) \tag{23}$$

$$NO + O \rightleftarrows O_2 + N \tag{24}$$

$$NO + N \rightleftarrows N_2 + O \tag{25}$$

where M represents any one of the five species. Assuming that Eq. (24) has a degree of disequilibrium value close to zero during the evolution of the chemical system, and the other four reactions have values far from zero, several different constraints for the RCCE method can be selected. For example, the constraints $\phi = NO + O_2$, $\phi = O + N$, and $\phi = NO + O - O_2 - N$ are some of the possibilities that represent summations that are not changed as the reaction $NO + O \rightleftarrows O_2 + N$ progresses, where ϕ is a summation of the number of moles of the indicated species. If several reactions have a DOD close to zero, then the number of constraints that could be chosen would be reduced.

The DOD constraint can be augmented by the fact that elements are conserved throughout the evolution of a chemical system (assuming no nuclear decay). For the above five-species air model, the following three equations represent the conservation of elemental oxygen, conservation of elemental nitrogen, and a constraint based on DOD analysis, respectively.

$$2\Delta O_2 + \Delta O + \Delta NO = 0 \tag{26}$$

$$2\Delta N_2 + \Delta N + \Delta NO = 0 \tag{27}$$

$$-\Delta O_2 - \Delta N + \Delta NO + \Delta O = 0 \tag{28}$$

where ΔI represents the change in the number of moles of species I during some amount of time. Equation (28) is generated by taking the stoichiometric coefficients from the reaction [Eq. (24)] that is in local equilibrium, and re-arranging the coefficients such that they sum to zero. Solving Eqs. (26–28) simultaneously results in two free parameters, as there are five equations and three unknowns. For example, $\Delta N_2 = (1/2)(3\Delta O_2 - \Delta NO)$, $\Delta O = -2\Delta O_2 - \Delta NO$, and $\Delta N = -3\Delta O_2$, if ΔO_2 and ΔNO are chosen to be the free parameters. This defines an infinite number of possible constraints that are based on the reaction $NO + O \rightleftarrows O_2 + N$ having a DOD value close to zero throughout the evolution of the chemical system, and augmented by considering the effects of elemental conservation. The free parameters can be chosen arbitrarily, and the method used to calculate this constraint for a specific problem is shown in Sec. VII.C.

VI. Overview of Air Test Cases

As very few previous studies exist that use the RCCE method to solve problems involving compressible flows, a detailed investigation into the performance of different constraints must be performed in order to understand if RCCE is a viable method for this flow regime. Two model test problems are used to accomplish this. Each case is set up in Cantera [41], using the Shock and Detonation Toolbox [36] to solve the reacting Euler equations. The appropriate thermodynamic data [42,43] and reaction rates [44] are found in the literature. Temperatures are kept under 6000 K so that there is a negligible concentration of ionized species in the gas mixture. Reactions shown in Eqs. (21–25) are used to model the air mixture that includes five species: N_2, O_2, NO, O, and N. The vector of mass fractions of the mixture, $\boldsymbol{Y}$, is defined to be $\boldsymbol{Y} = [Y_{N_2} \quad Y_{O_2} \quad Y_{NO} \quad Y_O \quad Y_N]^T$. The parameters for the test cases are chosen so that finite-rate chemical kinetics plays a role in determining the composition of the flow, and that the flow parameters are characteristic of what might be experienced in a hypersonic ground testing facility. One test case involves processing a gas mixture by a normal shock, and the other test case involves the steady expansion of a previously shocked gas. Not only are these two types of flows necessary for the operation of ground testing facilities, but also these two genres of flows are akin to what a blunt body would experience under reentry conditions: a bow shock over the forebody of the vehicle, and an expansion region as the flow turns around the shoulder of the body [2]. For all of the following work it is assumed that the gas is in thermal equilibrium; that is, translational/rotational/vibrational temperatures are assumed to be the same, and species diffusion will be neglected.

A. Case #1: Shocked Gas

For this test case, a gas mixture at 20 kPa and 297 K is processed by a normal shock traveling at 3 km/s. These initial conditions are very similar to Shot 2791 from T5 (hypervelocity shock tunnel located at the California Institute of Technology) [45], where a gas mixture at 22 kPa in the shock tube portion of the experimental facility was processed by a normal shock traveling at 3.1 km/s. However, the T5 gas mixture was primarily CO_2, and not air, for Shot 2791.

Across the normal shock, it is assumed that the composition of the flow remains frozen, but the gas behaves as an ideal gas where the relevant gas properties (γ, c_p, c_v, etc.) are a function of temperature. This assumption requires that the postshock state be solved for in an iterative manner, and Reynolds iterative method is used for this calculation [36]. After the postshock properties are calculated, the gas evolves kinetically until changes in the gas composition and thermodynamic properties are negligible. The results are shown in Fig. 1. Quantities are plotted as a function of distance in the shock fixed frame, where the shock is located at $x = 0$ m. In this example, the mixture compositions reached a relatively constant value at ~1 cm, which corresponds to ~25 μs downstream of the shock. Conditions for Case #1 are summarized in Table 1.

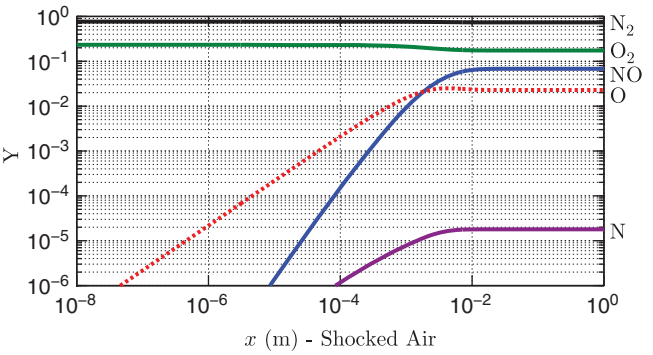

Fig. 1 Evolution of mass fractions for air at 20 kPa and 297 K processed by a 3 km/s ($M = 8.7$) normal shock.

Table 1 Initial and final gas properties for Case #1

Quantity	Initial conditions	Thermodynamic equilibrium conditions
$T(K)$	297	3457
P(kPa)	20	1853
Y_{N_2}	0.77	0.74
Y_{O_2}	0.23	0.17
Y_{NO}	0.00	0.068
Y_O	0.00	0.023
Y_N	0.00	0.000018

Table 2 Initial and final gas properties for Case #2

Quantity	Initial conditions	Conditions at area ratio = 17
$T(K)$	5,710	2,732
P(kPa)	17,300	192
Y_{N_2}	0.71	0.74
Y_{O_2}	0.042	0.16
Y_{NO}	0.11	0.058
Y_O	0.0048	0.043
Y_N	0.13	6.6×10^{-6}

Immediately behind the normal shock, the gas is in a state that is far from thermodynamic equilibrium, as it is at a high temperature and pressure, and it is not yet dissociated. Next, some of the N_2 and O_2 dissociates at this high-temperature and pressure condition. Farther downstream from the shock, a thermodynamic equilibrium state is reached, where T, P, and $\boldsymbol{Y}$ remain constant. As there is no imposed length scale on this problem, the point where thermodynamic equilibrium is reached is related only to the initial condition used for the problem (shock speed, initial pressure, and the gas mixture and model chosen). This case focuses on testing the RCCE method for a flow that starts far from thermodynamic equilibrium, and should eventually relax to a thermodynamic equilibrium state.

B. Case #2: Steady Expansion

For this test case, a gas mixture at high temperature and pressure is expanded through a 20° half-angle conical nozzle. The composition of this gas is calculated by taking the same initial conditions as in Sec. VI.A, then taking the equilibrium result from the original normal shock, and finally re-processing the gas again by a reflected shock. This approximates the conditions that would be seen in the reservoir of a reflected shock tunnel. To exaggerate the effect that finite rate kinetics have on the expansion, the gas mixture is taken to be the composition of the gas at the throat of the nozzle traveling at $M = 1$. In a real facility, the gas would accelerate to the sonic point through the converging aspect of the nozzle, and the temperature and pressure would both decrease as the velocity increases. The results are shown in Fig. 2, where the length is normalized by the nozzle diameter (2.54 cm). Conditions for Case #2 are summarized in Table 2.

This test case differs greatly from the previously discussed shock test case. First, the flow at the nozzle throat is in a thermodynamic equilibrium state. As the flow travels downstream, temperature and pressure decrease, which slow down the chemical reactions occurring. Eventually, the chemical reaction rates are so small that the gas composition remains relatively constant. This phenomenon is often referred to as nozzle freezing. From this point on, the flow is in a constant state away from a local equilibrium. In fact, the gas is in a state farther from thermodynamic equilibrium, the farther downstream the nozzle it travels. Nozzle freezing occurs at ~9 throat diameters downstream, which corresponds to an area ratio of ~17 in this problem. In addition, and contrary to the shock case (Sec. VI.A), a length scale is inherently imposed on this problem by choosing a nozzle geometry. This case focuses on testing the RCCE method for a flow that should reach a final state where the gas mixture is not in thermodynamic equilibrium, and this transition from equilibrium to nonequilibrium takes place over a finite length, imposed by the user.

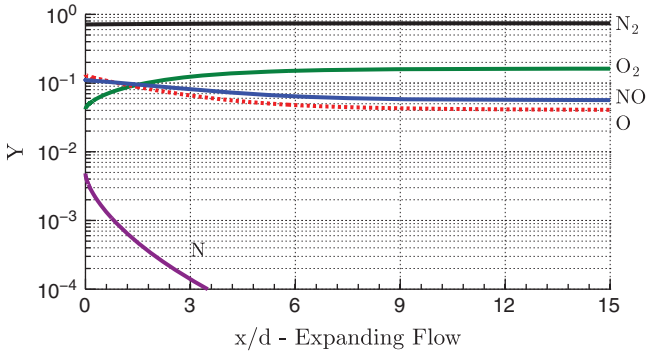

Fig. 2 Evolution of mass fractions for air originally in thermodynamic equilibrium at 5710 K and 17.3 MPa, undergoing a steady expansion.

VII. Constraint Selection

The constraints fall under three major categories: individual species constraints, global quantities, and constraints based on timescale analysis. The different constraints chosen in each category are outlined in the following sections, and are summarized in Table 3. Because of the relatively small chemical mechanisms considered in the following examples, this work is limited to using only one constraint. For more complicated chemical models, and depending on the level of accuracy desired by the user, it is possible that more than one constraint must be used, and this is common practice for the RCCE method. All of the work performed in the following sections could be extended to include more than one constraint, and should be the subject of future investigations.

A. Species Constraints

For completeness, each of the five species, O_2, N_2, O, N, and NO, is used as an individual constraint. In addition, the linear combination of the mass fractions of the major species ($O_2 + N_2$) and the linear combination of the mass fraction of the radical species (NO + O + N) are used as constraints. These are some of the original constraints suggested by Keck [14].

B. Global Quantities

Several "global quantities" of the gas mixture are also used as constraints. This is done by performing a weighted sum of the species mass fractions, in order to ensure that the desired quantity is reproduced perfectly. These quantities include the mixture molecular weight (previously used by Keck [14]) and the standard enthalpy of formation (summation of the enthalpy of formation of the species present, by mass), which is a new constraint. The enthalpy of formation is defined to be the change in enthalpy due to the formation of a molecule from its constituent elements at standard conditions. The mathematical formulations for these constraints are shown in Table 4, where $\Delta h^\circ_{f_i}$ is its enthalpy of formation (kJ/mol). The calculation of the molecular weight generally takes the form $\overline{W} = (\sum_{i=1}^{ns}(Y_i/W_i))^{-1}$. However, to define a constraint that is linear in mass fractions for the constrained equilibrium calculations, a choice of $\phi^8 = \sum_{i=1}^{ns} C_i^8 Y_i$ is used, where $C_i^8 = 1/W_i$. This results in $\phi^8 = 1/\overline{W}$. The global constraints are listed in Table 4.

C. Constraints Based on DOD Analysis

Figures 3a and 3b show the results when the DOD analysis presented in Sec. V.B is applied to both test cases. This following analysis is similar to previous approaches that have been used to determine DOD constraints for the RCCE method [31,32]. The sign of the value of DOD in general switches between the two cases, as dissociation reactions are more prevalent in the shocked flow, while recombination reactions dominate the nozzle flow. In both cases, it can be seen that for at least one of the five reactions (different in each case), the forward and reverse reaction rates remain essentially equal throughout the system. In the shocked case, it is $N + O + M \rightleftarrows NO + M$, whereas in the nozzle flow, it is $NO + O \rightleftarrows O_2 + N$. As different reactions have a DOD value of

Table 3 Summary of constraints to be investigated in this section

Category	Constraint name	k	$\phi^k = \sum_{i=1}^{ns} C_i^k Y_i$	Same C_i's for shock and nozzle (Y/N)
Species constraints	Major species	1	$C^1_{N_2,O_2} = 1, C^1_{NO,O,N} = 0$	Y
	Radical species	2	$C^2_{N_2,O_2} = 0, C^2_{NO,O,N} = 1$	Y
	N_2	3	$C^3_{N_2} = 1, C^3_{i\neq N_2} = 0$	Y
	O_2	4	$C^4_{O_2} = 1, C^4_{i\neq O_2} = 0$	Y
	NO	5	$C^5_{NO} = 1, C^5_{i\neq NO} = 0$	Y
	O	6	$C^6_{O} = 1, C^6_{i\neq O} = 0$	Y
	N	7	$C^7_{N} = 1, C^7_{i\neq N} = 0$	Y
Global quantities	Inverse molecular weight	8	$C_i^8 = Y_i/W_i$	Y
	Enthalpy of formation	9	$C^9_{N_2,O_2} = 0$, $C^9_{NO} = (\Delta h^\circ_{f_{NO}}/W_{NO})Y_{NO}$, $C^9_{O} = (\Delta h^\circ_{f_O}/W_O)Y_O$, $C^9_{N} = (\Delta h^\circ_{f_N}/W_N)Y_N$	Y
Timescale analysis	Fast mode	10	$C_i^{10} = \overline{\nu_i^*}$	N
	DOD #1	11	See Sec. VII.C	N
	DOD #2	12	See Sec. VII.C	N

For $k = 8$, the conversion from mole fractions to mass fractions requires that the inverse of molecular weight be used to keep the constraint linear in mass fractions, and for $k = 11$ and $k = 12$, more analysis is needed to determine the appropriate constraint coefficients.

Table 4 Global constraint examples

Global property	Constraint
Molecular weight	$\phi^8 = (Y_{N_2}/W_{N_2}) + (Y_{O_2}/W_{O_2}) + (Y_{NO}/W_{NO}) + (Y_O/W_O) + (Y_N/W_N)$
Enthalpy of formation	$\phi^9 = (\Delta h^\circ_{f_{NO}}/W_{NO})Y_{NO} + (\Delta h^\circ_{f_O}/W_O)Y_O + (\Delta h^\circ_{f_N}/W_N)Y_N$
	$\Delta h^\circ_{f_{NO}} = 90$ kJ/mol, $\Delta h^\circ_{f_O} = 247$ kJ/mol, $\Delta h^\circ_{f_N} = 471$ kJ/mol

The enthalpies of formation for O_2 and N_2 are zero and are not included in the general enthalpy of formation calculation.

close to 0 in the two cases considered, this indicates that it will likely be challenging to find one DOD constraint that will work for both shocks and expansions. These reactions will be combined with elemental conservation to determine the constraint to be used.

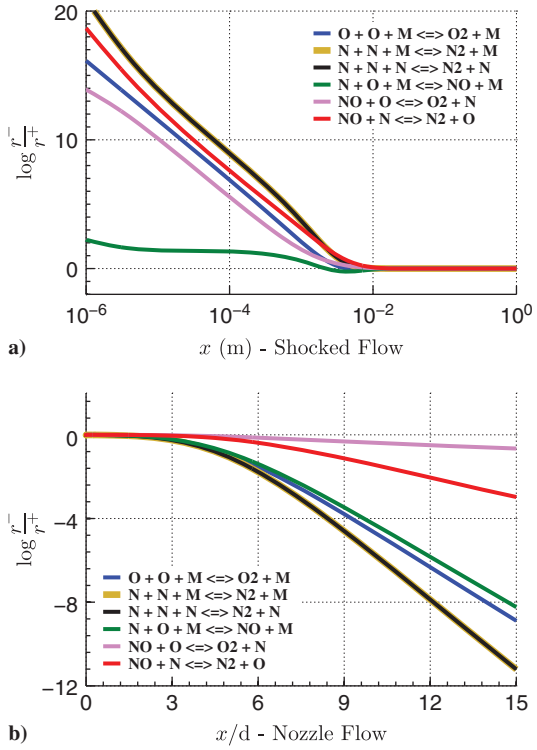

Fig. 3 Degree of disequilibrium calculation for each reaction considered in the air system for Case #1 (a) and Case #2 (b).

Following the same method outlined in Sec. V.B, constraints are calculated for both test cases. For the shock case, one set of solutions is $\Delta N_2 = (1/4)(2\Delta O_2 - 3\Delta N)$, $\Delta NO = (1/2)(-2\Delta O_2 + \Delta N)$, and $\Delta O = -(\Delta O_2 + (\Delta N/2))$, where ΔO_2 and ΔN are chosen to be the free parameters. For the nozzle case, one set of solutions is $\Delta N_2 = (1/2)(3\Delta O_2 - \Delta NO)$, $\Delta O = -2\Delta O_2 - \Delta NO$, and $\Delta N = -3\Delta O_2$, where ΔO_2 and ΔNO are chosen to be the free parameters.

The constraints calculated through the degree of disequilibrium analysis combined with element conservation are summarized in Table 5. Two possible constraints are shown for each test case, as it is possible to vary the free parameters and create a different constraint. The arbitrariness involved with selecting free parameters is not desirable when trying to derive a constraint in a rigorous manner. It will be shown that this subjectivity in constraint selection does have an impact on the performance of the constraint and, hence, reduces the applicability and generality of DOD-based constraints. Values for the free parameters are chosen to be of order 1, in order to stay consistent with the other constraints described in this section.

Beretta et al. have automated much of the DOD constraint selection methodology in a recent work [31]. However, there still remains some amount of user intuition and insight required based on how the different reactions group together based on their DOD values. In addition, the user must still define an appropriate number of constraints to use for a given problem. Although constraints based on DOD work well for some cases, it will be shown in the following sections that, due to subjectivity in constraint selection and the fact that different reactions have a DOD value close to 0 for the shock and nozzle test cases, a constraint based on the DOD analysis is not preferred for the current investigation.

D. Constraints Based on Timescale Analysis

Using the method outlined in Sec. V.A, the different reaction modes and associated timescales are analyzed for the two test cases. For the present five-species air mixture, ns = 5 and ne = 2. Hence, three (ns − ne) reaction modes and timescales can be calculated from the Jacobian matrix [Eq. (20)]. The modes are ordered such that

Table 5 Selected constraints based on degree of disequilibrium analysis

Test case	Chosen reaction	k	Free parameters	Constraint
Expanding flow	$NO + O \rightleftarrows O_2 + N$	11	$X_{O_2} = 2, X_{NO} = 1$	$\phi^{11}_{Nozzle} = (5/2)(Y_{N_2}/W_{N_2}) + 2(Y_{O_2}/W_{O_2}) + (Y_{NO}/W_{NO}) - 5(Y_O/W_O) - 6(Y_N/W_N)$
		12	$X_{O_2} = 3, X_{NO} = 2$	$\phi^{12}_{Nozzle} = (7/2)(Y_{N_2}/W_{N_2}) + 3(Y_{O_2}/W_{O_2}) + 2(Y_{NO}/W_{NO}) - 8(Y_O/W_O) - 9(Y_N/W_N)$
Shocked flow	$N + O \rightleftarrows NO$	11	$X_{O_2} = 1, X_N = 0$	$\phi^{11}_{Shock} = (1/2)(Y_{N_2}/W_{N_2}) + (Y_{O_2}/W_{O_2}) - (Y_{NO}/W_{NO}) - (Y_O/W_O)$
		12	$X_{O_2} = 2, X_N = 1$	$\phi^{12}_{Shock} = (1/2)(Y_{N_2}/W_{N_2}) + 2(Y_{O_2}/W_{O_2}) - (3/2)(Y_{NO}/W_{NO}) - (5/2)(Y_O/W_O) + (Y_N/W_N)$

Two possible constraints (DOD #1 and DOD #2) are shown for each test case.

$t^*_1 < t^*_2 < t^*_3$. Figures 4a and 4b show the evolution of the normalized timescales for the two test cases. As a point of reference, at $x/d = 2$, $t^*_1 \approx 5 \cdot 10^{-9}$ s, $t^*_2 \approx 5 \cdot 10^{-7}$ s, and $t^*_3 \approx 1.3 \cdot 10^{-6}$ s. These times should be compared with the relevant fluid mechanical timescales. For a nozzle, this can be estimated from $t^*_{flow} \approx ((U/P)(dP/dx))^{-1}$. (Professor Joe Shepherd, Notes of March 9, 2013, "Simplified timescale analysis for reacting flow using Jacobian eigen-analysis."). At $x/d = 2$, $t^*_{flow} \approx 1.5 \cdot 10^{-5}$.

Figures 4a and 4b show that, although there is a significant timescale separation between mode one and the other two reaction modes, modes two and three have similar characteristic times. This result holds for both the shocked flow and the expanding flow. The fastest reaction mode represents a linear combination of some or all of the original five reactions [Eqs. (21–25)]. As this mode equilibrates quicker than the other two modes in the system, this "pseudo" reaction should not affect the value of the chosen constraint. This is a similar argument that was used for the DOD method, except that the reaction mode is used instead of one individual reaction from the original chemical mechanism.

Figures 5a and 5b show the evolution of the fastest reaction mode (mode one) for each test case, where ν^*_i is the coefficient taken from the eigenvector associated with the fastest reaction mode (molar based), for species i. All coefficients are normalized by $\nu^*_{O_2}$. For both cases, the reaction coefficients remain relatively constant throughout the system. It should be noted that, for small distances behind the shock ($x < 10^{-3}$ m, not plotted) in Case #1, eigenvalues with positive real components are observed. This identifies reaction modes where perturbations parallel to this mode would not relax to the initial composition, but instead would move farther away from the initial state. These positive eigenvalues are attributed to the state of the shocked air system immediately downstream of the shock, where the high-temperature nondissociated gas mixture is very far from an equilibrium composition. The presence of these positive eigenvalues shows that, while being an interesting theoretical concept, it is often difficult to apply a timescale analysis used in methods like CSP and ILDM to practical systems.

Some practical issues arise when calculating numerical values for a constraint based on the fastest reaction mode. First, as the solution evolves, neither the reaction modes nor the characteristic timescales remain constant. The separation between the characteristic time associated with the fastest and slower modes is consistent throughout both cases, but the changing value of the reaction mode implies that a nonconstant constraint should be used when combined with RCCE. Second, these constraints are not consistent between the shocked flow and expanding flow scenarios, due to the fundamentally different physical phenomena that occur in each case. After extensive testing, although the nonconstant reaction coefficients were found to have some effect on the calculated results, using average reaction coefficients was found to give adequate results. Third, and similar to DOD discussion presented previously, if more than one constraint were to be used for a fully integrated RCCE simulation, the user would have to decide how many reaction modes to include, which

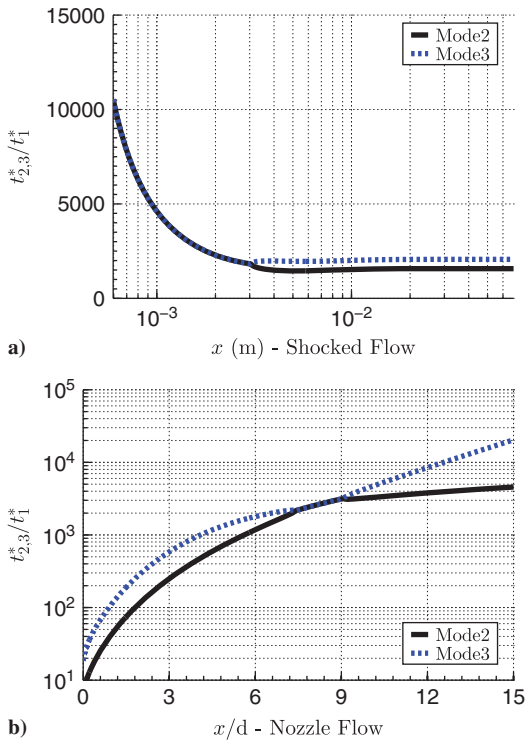

Fig. 4 Evolution of the normalized reaction mode timescales for shocked flow a) and expanding flow b).

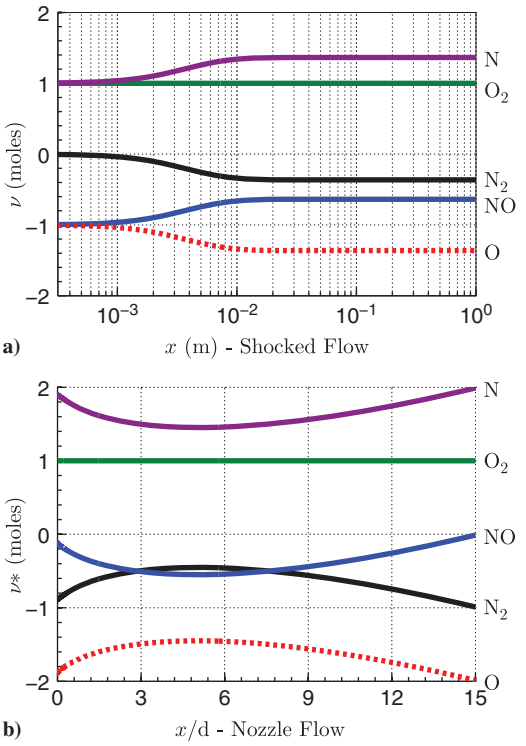

Fig. 5 Evolution of the reaction coefficients for Case #1 a) and Case #2 b) for the fast reaction mode in air, normalized by ν_{O_2}.

adds some level of arbitrariness to this method. Finally, when a tabulated method is used for the constraints, this timescale analysis need to be performed only once, off line, before running a fully integrated RCCE simulation.

For the constraint based on the fast reaction mode (ϕ^{10}), the coefficients, C_i^{10}, are chosen to be $C_i^{10} = \overline{\nu_i^*}$, yielding $\phi^{10} = \sum_{i=1}^{ns} \overline{\nu_i^*}\, Y_i$, where $\overline{\nu_i^*}$ is the average ith reaction coefficient (mass fraction based) for the fastest reaction mode. The average (to calculate $\overline{\nu_i^*}$ from $\boldsymbol{\nu}_i^*$) is performed over the domain where the eigenvalue associated with the fastest reaction mode is negative, and reactions are still occurring. All values of $\overline{\nu_i^*}$ are normalized such that $\overline{\nu_{O_2}^*} = 1$. For the shocked flow, the average is performed over the range 3.17×10^{-4} m $< x < 10^{-2}$ m, and for the nozzle flow, the average is performed over $0 < x/d < 9$. The values for $\overline{\boldsymbol{\nu}^*}$ are *not* the same for both the shock and nozzle cases. Calculating these averages results in $\overline{\boldsymbol{\nu}^*_{\text{Shock}}} = [-0.20, 1, -0.72, -0.61, 0.53]^T$, and $\overline{\boldsymbol{\nu}^*_{\text{Nozzle}}} = [-0.46, 1, -0.44, -0.76, 0.67]^T$, for the shocked and nozzle flow, respectively, where $\boldsymbol{Y} = [Y_{N_2}, Y_{O_2}, Y_{NO}, Y_O, Y_N]^T$. This results in

$$\phi^{10}_{\text{Shock}} = \sum_{i=1}^{ns} \overline{\nu^*_{\text{Shock},i}}\, Y_i \tag{29}$$

and

$$\phi^{10}_{\text{Nozzle}} = \sum_{i=1}^{ns} \overline{\nu^*_{\text{Nozzle},i}}\, Y_i \tag{30}$$

VIII. Constraint Performance

The different aforementioned constraints are implemented and compared with the results from the Cantera simulations obtained with detailed chemistry. To gain insight into the effectiveness of each constraint, the effect of error propagation that would be present in a fully coupled simulation is removed by comparing the detailed chemistry simulation results with RCCE results at every point in the flow. Results pertaining to fully integrated simulations will be shown later, in Sec. IX.

A. Comparison Methodology

For each test problem, four basic plots are used to reveal how a constraint behaves through the system. Only two sample examples are included in this work (Figs. 6 and 7), whereas a more detailed analysis of each constraint can be found elsewhere [46]. First, the constraint ϕ is plotted as a function of a spatial coordinate, showing how the constraint evolves through the reacting system (top left). The value of ϕ is calculated based on the detailed chemistry results, and one constraint is used in all cases. For the remaining three plots, quantities are plotted as a function of ϕ [Eq. (12)]. As the RCCE method requires the system to be reconstructed as a function of ϕ, this is the appropriate space to visualize and evaluate the efficacy of the constraints.

The second plot (top right) shows the species mass fractions as a function of ϕ. Values calculated from the detailed chemistry simulations, $\boldsymbol{Y}$, are labeled as "Cantera," and are compared with values calculated from constrained thermodynamic calculations, $\boldsymbol{Y}^{\text{CEQ}}$ [Eq. (13)], where the constrained equilibrium calculations are based on the T, P, and ϕ generated from the detailed chemistry results. All discrepancies in the mixture properties between the Cantera results and the CEQ results can be attributed to differences between $\boldsymbol{Y}$ and $\boldsymbol{Y}^{\text{CEQ}}$.

As discussed in Sec. IV, when coupled with a CFD solver, the bulk properties of the fluid mixture are needed. γ, the ratio of specific heats, is taken to be a characteristic bulk property. Constrained equilibrium calculation results (γ^{CEQ}) are compared with detailed chemistry results (γ) in the third plot (bottom left). Finally, not only is it necessary to transport the value of ϕ in an integrated simulation, but also the source term for the constraint, $\partial\phi/\partial t$, must also be known as a function of ϕ. The final plot (bottom right) compares $|\partial\phi^{\text{CEQ}}/\partial t|$ [Eq. (15)] and $|\partial\phi/\partial t|$ [Eq. (16)]. Depending on the choice of constraint, all or only some of the reactions from the full mechanism are used. The absolute value of this function is compared between the two cases (for visualization purposes). The enthalpy of formation constraint is used in Figs. 6 and 7 as this constraint was found to perform best overall. Figures 6 and 7 show that ϕ increases in Case #1 as a function of distance, whereas it decreases in Case #2. Additionally, it can be seen from Fig. 7 that even relatively small errors made on mass fractions can result in noticeable errors on $|\partial\phi/\partial t|$, as reaction rates associated with reactions that are close to being in equilibrium are sensitive to relatively small changes in mass fractions.

B. Analysis of Constraint Performance

In this section, quantitative error calculations are presented. A comparison of γ, the ratio of specific heats, was shown graphically in Figs. 6 and 7. For an ideal gas, γ is related both to the molecular weight ($\overline{W}$) and the heat capacity (c_p) of a mixture; $\gamma = (c_P/(c_{p-R}))$,

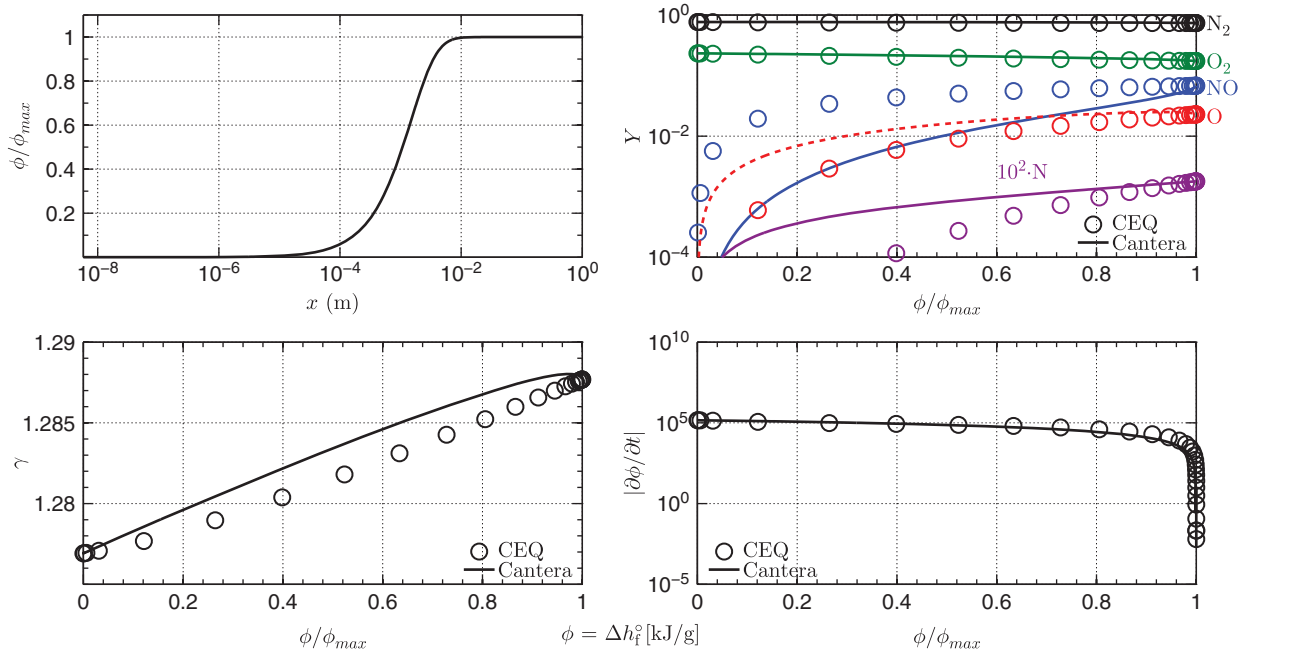

Fig. 6 Finite-rate chemistry and constrained equilibrium calculations for a shocked air flow. Constrained equilibrium calculations are performed by holding the enthalpy of formation (by mass) of the mixture constant (constraint #9).

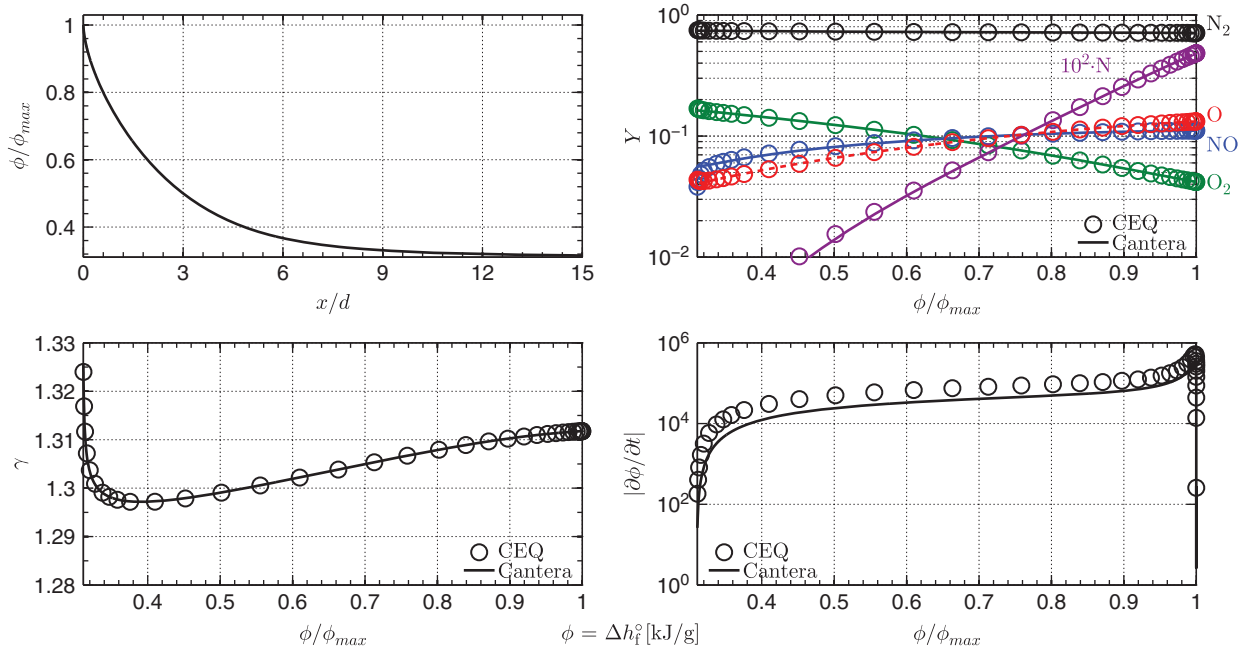

Fig. 7 Finite-rate chemistry and constrained equilibrium calculations for an expanding air flow. Constrained equilibrium calculations are performed by holding the enthalpy of formation (by mass) of the mixture constant (constraint #9).

where R is the specific gas constant ($R = (\mathcal{R}/\overline{W})$), and $\mathcal{R}$ is the universal gas constant. As such, even though γ does not appear explicitly in Eqs. (5–8), a comparison of γ encompasses errors from both the molecular weight of the mixture, and from the c_p of the mixture. In addition, comparing γ evaluates errors that are associated with the $\int_{T_o}^{T} c_{p,i}(T')\,dT'$ term in the $h_i(T_o)$ calculation previously mentioned [Eq. (11)]. The reference enthalpy of the mixture ($h(T_o) = \sum_{i=1}^{\text{ns}} Y_i h_i(T_o)$) is another logical choice of a bulk property to compare, due to the appearance of the h_i terms in Eq. (10). The reference enthalpy is used in order to place an emphasis on the error made in mass fractions between the two computational methods. Finally, a comparison of the source term, $\partial\phi/\partial t$, gives an indication of how the system would evolve.

For this work, an L_2 norm is defined to compare the different constraints. If an arbitrary fluid property, F, is chosen, then

$$L_{2,w}^k = \left[\frac{1}{\phi_{\max}^k - \phi_{\min}^k}\sum_{l}^{N}\Delta\phi_l^k |F(\phi_l^k) - F^{\text{CEQ}}(\phi_l^k)|^2\right]^{1/2} \tag{31}$$

where N is the number of points used in the calculation, l represents a point in the flow, k corresponds to the specific constraint being compared (see Table 3), $\Delta\phi_l^k$ is the local grid spacing in ϕ^k ($\Delta\phi_l^k = (\phi_{l+1}^k - \phi_{l-1}^k)/2$), and $\phi_{\max}^k$ and $\phi_{\min}^k$ are the maximum and minimum values of ϕ^k in the domain, respectively. $F(\phi_l^k)$ [e.g., Eq. (18)] corresponds to a mixture property calculated from detailed chemistry simulations, and $F^{\text{CEQ}}(\phi_l^k)$ [e.g., Eq. (17)] corresponds to a mixture property calculated at the same point in the flow, but using constrained equilibrium calculations, for the kth constraint.

Figures 8 and 9 compare the performance of the different constraints in a quantitative manner. Results for γ and $h(T_o)$ are shown in Fig. 8 and are normalized by the maximum error in each test case, that is, the maximum error over all k for a specific test case, so that all error calculations range from 0 to 1. The results for $\partial\phi/\partial t$ are shown in Fig. 9. Here, each individual data point is normalized by the local max($|\partial\phi/\partial t|$), that is, the maximum value of $|\partial\phi/\partial t|$ for a specific k, in order to estimate the order of magnitude of error expected if the source term were to be used to reconstruct the original ϕ profile. Different constraints are shown on the x axis (varying k), and their respective norms are plotted vertically. Each vertical column portrays how an individual constraint performs. Symbols closer to the x axis indicate a smaller norm magnitude, and therefore a smaller difference between the CEQ results and the detailed chemistry results.

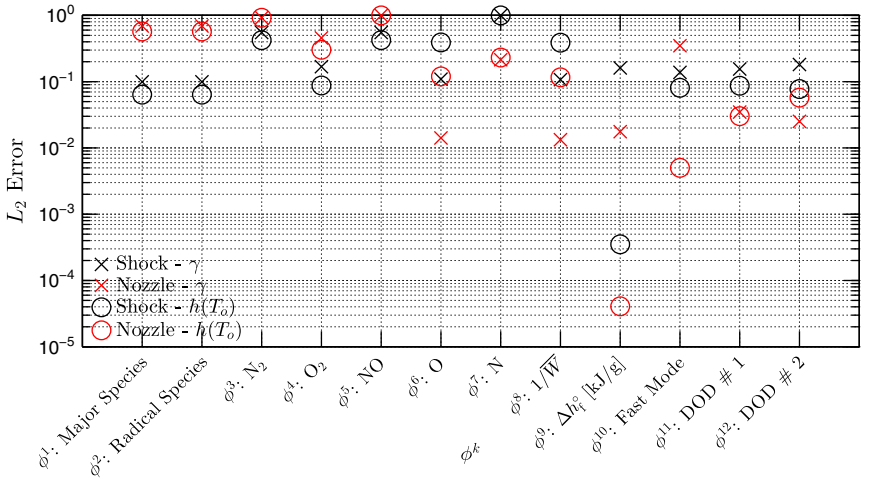

Fig. 8 L_2 error for $h(T_o)$ and γ, calculated from Eq. (31). Each data set is normalized by the maximum error from the respective test case. Different constraints are shown on the x axis (varying k), and their respective norms are plotted vertically.

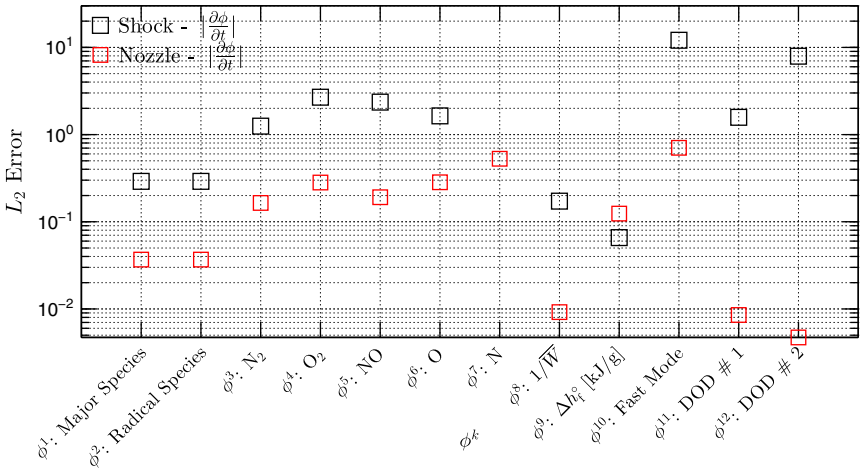

Fig. 9 L_2 error for the source term. $|\partial\phi/\partial t|$ values are calculated from Eq. (31). Calculated errors are individually normalized by $\max(|\partial\phi/\partial t|_{\text{Cantera}})$ in each trial, respectively. Different constraints are shown on the x axis (varying k), and their respective norms are plotted vertically.

As mentioned in Sec. VII.C, it is apparent from Figs. 8 and 9 that the chosen free parameters in the degree of disequilibrium analysis can affect the accuracy of the results obtained with this constraint. Figure 9 also shows that the DOD constraints perform much better for the nozzle test case than for the shock test case. The current results are consistent with the results reported in [31,32], but show that care must be taken when applying this constraint to different systems.

In general, from Figs. 8 and 9 it can be seen that constraining the enthalpy of formation consistently performs well for both the nozzle and shock simulations. Although constraining on the enthalpy of formation is expected to perform well for reproducing the mixture enthalpy, its performance as it pertains to γ is similar (if not better) to any other constraint. In addition, as the enthalpy of formation is a global property of a mixture, this constraint is the same between the two test cases (shock and nozzle), and no a priori knowledge of the underlying chemical model is necessary. It is a constant constraint that can be used when either dissociation or recombination reactions are dominant. In the air system considered, it corresponds to a weighted sum of the radical species present. This constraint performs well because the radical species are associated with fast timescales, which is the fundamental idea of RCCE; weighting the radicals based on their enthalpy of formations assures that the relevant bulk properties of the mixture are as accurate as possible. This constraint has not received any attention in the literature for previously performed calculations involving RCCE.

To take these results one step further, the evolution of ϕ can be reconstructed by integrating the $\partial\phi^{\text{CEQ}}/\partial t$ values calculated in the previous section. This reconstructed value of the constraint will be referred to as ϕ^{RCEQ}, and will be calculated only for ϕ^9, the constraint based on the enthalpy of formation. By calculating ϕ^{RCEQ} in this manner, no feedback from T or P is considered. As $(\partial\phi^{\text{CEQ}}/\partial t) = f(\phi)$ (where $f(\phi)$ is plotted in Figs. 6 and 7), it follows that $\int_{t_o}^{t} \mathrm{d}t' = \int_{\phi_o}^{\phi} \partial\phi'^{\text{CEQ}}/f(\phi')$. This is integrated numerically to solve for $\phi^{\text{RCEQ}}(t)$, with $t_o = 0$ and $\phi_o = \phi(t_o)$. The results of this reconstruction are shown in Fig. 10a for the shock case, and in Fig. 10b for the nozzle case, where ϕ and ϕ^{RCEQ} are plotted. Figures 10a and 10b represent a simple integration of Figs. 6 and 7.

As shown in Fig. 9, the relative error on $|\partial\phi/\partial t|$ is approximately 20% for the nozzle case, and approximately 1% for the shock case. Although the two reconstructions reach the same final value of ϕ, there is approximately a 50% difference around $t \approx 30$ μs in the nozzle case (Fig. 10b). The error is much smaller in the shock case, and the reconstruction is much more accurate, as shown in Fig. 10a. This error in the nozzle case could imply that a different state is reached at intermediate locations in the nozzle, which could correspond to discrepancies downstream in the nozzle when nozzle freezing is expected to occur. A fully integrated simulation needs to be performed in order to fully evaluate the errors induced in this case.

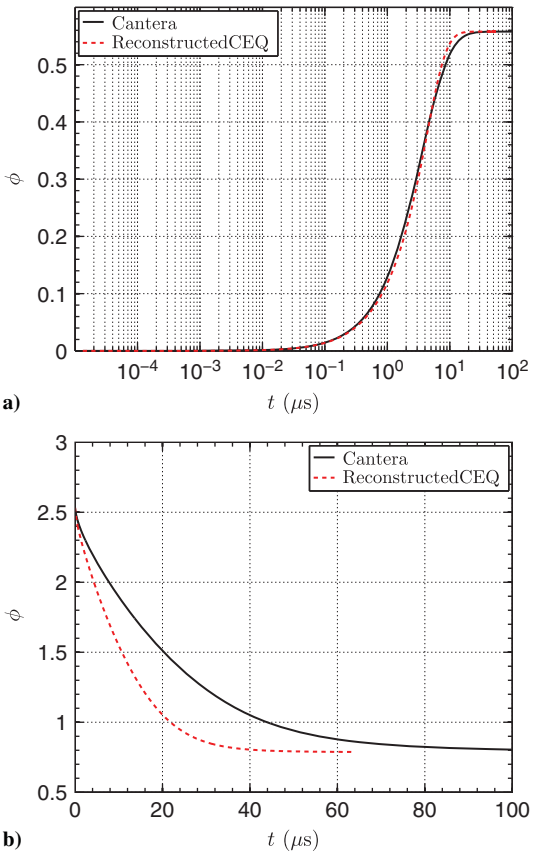

Fig. 10 Comparison between ϕ^{RCEQ} and ϕ calculated from detailed chemistry simulations, plotted as a function of time for a) the shock case and for b) the nozzle case. The calculations are performed for ϕ^9, a constraint based on the enthalpy of formation, and represent a simple integration of Figs. 6 and 7.

IX. Integrated RCCE Simulations

To confirm that the results shown in Sec. VIII.B remain valid when the full RCCE method is used, an integrated simulation is performed for the shock and nozzle test cases using a single constraint on the enthalpy of formation. The term "integrated simulation" is used to imply that feedback from T and P is included in the simulation. To couple the RCCE method with a CFD solver in an efficient manner, a tabulated approach can be used. This is a method that is widely used in computational chemistry (e.g., see [47,48]). Before running an integrated CFD simulation, tables are created with precalculated values of mass fractions ($\boldsymbol{Y}^{\text{CEQ}}$) as a

function of T, P, and ϕ^9. The following sections outline how the integrated simulations are performed and show the results of these simulations.

A. Methodology for RCCE Simulations

Knowing that a tabulation method based on temperature and pressure will be used, the 1D reacting Euler equations [Eqs. (5–8)] must be re-written in a manner consistent with this choice, and the species equations must be replaced with an equation for ϕ^9. The superscript 9 will no longer be used with ϕ, as this section considers only ϕ^9, the constraint based on the enthalpy of formation.

With one constraint, an expression for $(\mathrm{d}\phi/\mathrm{d}x)$ is required. Properties calculated from the fully integrated RCCE simulation will now take the superscript R. We start with

$$\frac{\partial \phi^R}{\partial t} = \sum_{i=1}^{\mathrm{ns}} C_i \frac{\partial Y_i^R}{\partial t} = \sum_{i=1}^{\mathrm{ns}} C_i \Omega_i(T^R, P^R, \boldsymbol{Y}^R) = \frac{\partial \phi^R}{\partial t}(T^R, P^R, \phi^R) = \dot{\phi}^R \tag{32}$$

This simplifies to

$$\frac{\mathrm{d}\phi^R}{\mathrm{d}x} = \frac{\dot{\phi}^R}{\mathrm{w}} \tag{33}$$

which replaces Eq. (8). The calculation of Y_i^R will be discussed in Sec. IX.B, and is based on a tabulated approach.

To keep the system of equations consistent with the tabulation method (as a function of T, P, ϕ) to be used, Eq. (5) must be substituted for an evolution equation for temperature. Following the derivations performed in [35], one can show that

$$\frac{\mathrm{d}T}{\mathrm{d}x} = \frac{T}{\mathrm{w}}\left[(1-\gamma M^2)\frac{\dot{\sigma}}{\eta} - \sum_{i=1}^{\mathrm{ns}} \frac{\overline{W}}{W_i}\dot{\Omega}_i\right] \tag{34}$$

This can be generalized to include an area change if desired, as shown by Kao and Shepherd [35].

All of the equations needed for the RCCE simulation can now be written as

$$\frac{\mathrm{d}\mathrm{w}^R}{\mathrm{d}x} = \frac{\dot{\sigma}^R}{\eta^R} \tag{35}$$

$$\frac{\mathrm{d}P^R}{\mathrm{d}x} = -\rho^R \mathrm{w}^R \frac{\dot{\sigma}^R}{\eta^R} \tag{36}$$

$$\frac{\mathrm{d}T^R}{\mathrm{d}x} = \frac{T^R}{\mathrm{w}^R}\left[(1-\gamma^R(M^R)^2)\frac{\dot{\sigma}^R}{\eta^R} - \sum_{i=1}^{\mathrm{ns}} \frac{\overline{W}^R}{W_i}\dot{\Omega}_i^R\right] \tag{37}$$

$$\frac{\mathrm{d}\phi^R}{\mathrm{d}x} = \frac{\dot{\phi}^R}{\mathrm{w}} \tag{38}$$

To solve Eqs. (35–38), a method to determine $\boldsymbol{Y}^R(T^R, P^R, \phi^R)$ is required, as $\dot{\sigma}^R$, η^R, ρ^R, γ^R, $\overline{W}^R$, $\dot{\Omega}_i^R$, and $\dot{\phi}^R$ are all functions of $\boldsymbol{Y}^R$. This is discussed in the next section.

B. Tabulated Approach

It is possible to calculate $\boldsymbol{Y}^R(T^R, P^R, \phi^R)$ from constrained thermodynamic equilibrium calculations, assuming that T^R, P^R, and ϕ^R are known (see Sec. IV). Instead of having to perform a Gibbs function minimization calculation at every point in the flow, values for $\boldsymbol{Y}^R(T^R, P^R, \phi^R)$ are tabulated before running a simulation. A 3-dimensional table is created, which includes 100 different values for P, T, and ϕ, respectively. The table contains 10^6 points in total. In each respective dimension, the points are linearly spaced between the minimum and maximum values considered. For the same table to be used for both the shock and nozzle test cases, a relatively large range of temperature, pressure, and ϕ is required. Hence, the minimum and maximum values chosen are 39 kPa and 17.5 MPa, 2000 and 5800 K, and 0 and 2.6 kJ/g, for pressure, temperature, and ϕ, respectively. This covers the minimum temperature, pressure, and ϕ range necessary for both the shock and nozzle test cases. When solving Eqs. (35–38), after each iteration, $\boldsymbol{Y}^R(T^R, P^R, \phi^R)$ is taken from the table, using a simple tri-linear interpolation method to interpolate values inside of the table. The results were found to be insensitive to table resolution, and all results presented in the next section use the table with 10^6 points.

C. Integrated Simulation Results: Shock

Results are shown for the mass fraction evolution and the value of the constraint for the shock test case in Figs. 11a and 11b, respectively. The evolution of ϕ (Fig. 11b), which includes feedback from T and P, is very similar to the earlier results shown in Fig. 10a, where no T and P feedback was considered. This is to be expected, as the variations in temperature and pressure behind the shock are relatively small. Figure 11a shows that some errors are made on the radical species initially (over prediction of NO, and an under prediction of O and N), but both the RCCE solution and the detailed chemistry solution tend to an extremely similar equilibrium state. Only minor variations are observed between the detailed chemistry results and the RCCE results; differences of ∼100 Pa, ∼3 K, and ∼0.002 kJ/g are observed at $x = 1$ m for pressure, temperature, and ϕ, respectively. The maximum error in mass fractions at $x = 1$ m is made on Y_{O_2}, and is ∼0.002. Only very small errors are expected, as the RCCE method is based heavily on thermodynamics, and should be accurate for flows reaching thermodynamic equilibrium. The final discrepancies are most likely caused by errors induced through tabulation, and from deviations of the RCCE solution and the detailed chemistry solution behind the shock.

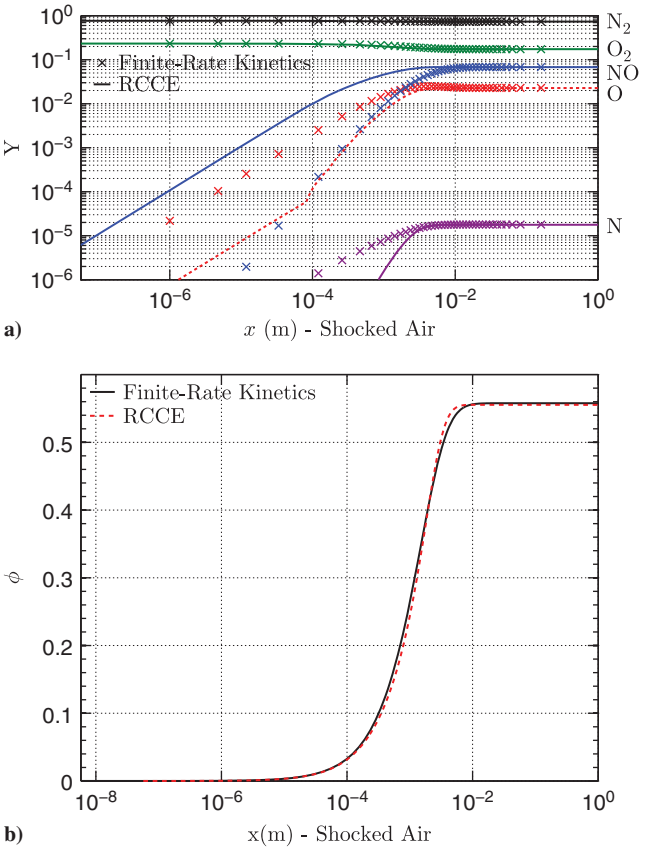

Fig. 11 Results for a fully integrated simulation using the RCCE method for the shock test case, constraining on enthalpy of formation. a) Mass fraction evolution; b) evolution of the constraint.

Although small errors are observed on individual mass fractions in the shock case, these errors do not have a large effect on the evolution of the source term (Fig. 11b). To increase the accuracy of the method it is possible to add additional constraints, though this increases the computational complexity of the problem as an additional equation must be solved, and an additional dimension must be added to the tabulation procedure.

D. Integrated Simulation Results: Nozzle

Results are shown for the mass fraction evolution and the value of the constraint for the nozzle test case in Figs. 12a and 12b, respectively. As expected, due to the overestimation of the source term seen in Fig. 10a, the RCCE simulation reaches a slightly different final composition before freezing occurs in the nozzle. Overall, there is good agreement between the two simulations. At $x/d = 15$, errors of ~150 K, ~720 Pa, and ~0.2 kJ/g are made on temperature, pressure, and ϕ, respectively, between the two simulations. The largest discrepancy in mass fractions at $x/d = 15$ is found to occur on Y_{O_2}, with a difference of ~0.02.

When comparing Fig. 12b with Fig. 10b, it is interesting to see that the fully integrated RCCE simulation compares better to the original simulation performed with finite-rate kinetics than the reconstructed solution calculated in Sec. VIII.B. It is postulated that this "self-healing" effect can be explained by considering the basic physics involved with reacting nozzle flow. Under supersonic conditions, as the flow travels downstream in the nozzle, the pressure and temperature of the flow decrease, whereas the Mach number increases. As temperature and pressure decrease, the formation of major species (fewer radical species) is favored from a thermodynamic point of view. These recombination reactions are exothermic, and add heat to the flow.

In Fig. 10b, ϕ^{RCEQ} is predicted to decrease too quickly as the flow travels through nozzle (when compared with the detailed chemistry solution). As the enthalpy of formation is used as the constraint, this corresponds to the RCCE simulation overpredicting the number of recombination reactions, which causes the temperature of the gas mixture to also be overpredicted. This overprediction of temperature then drives the RCCE simulation back toward the detailed chemistry solution, as the overprediction in temperature favors the formation of radical species from a thermodynamic standpoint. This does not occur in the reconstructed test case because T and P feedback are not included, and the reconstructed solution continues to diverge from the detailed chemistry solution.

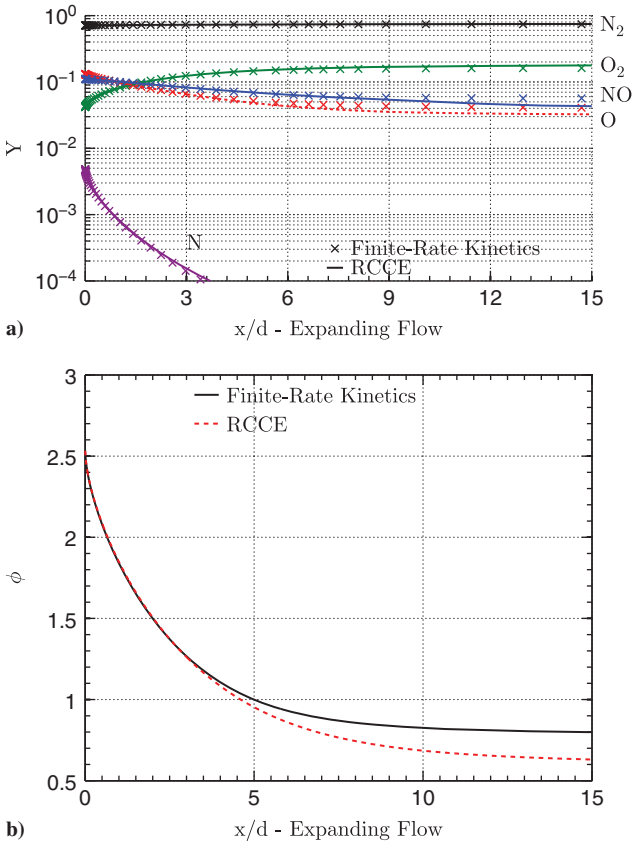

Fig. 12 Results for a fully integrated simulation using the RCCE method for the nozzle test case, constraining on enthalpy of formation. a) Mass fraction evolution; b) evolution of the constraint.

E. Discussion

To evaluate whether this method is desirable for a more detailed simulation (potentially 2D or 3D), some consideration should be given to the desired application of the RCCE method. In situations where it is not a priority to perfectly resolve a mixture composition, the RCCE method is advantageous. For the shock case, the RCCE method captures some of the nonequilibrium effects of the flow occurring, tends toward the correct final equilibrium state, and adds only a minimal amount of additional complexity when compared with a nonreacting flow simulation. On the other hand, for applications where the composition of the flow must be known immediately downstream of a shock, then the errors observed in Fig. 11a may be too large. In the nozzle case, Fig. 12a shows that the RCCE method was more accurate closer to the nozzle throat, where the flow was closer to being in a state of local equilibrium, and larger errors were observed farther downstream, when the flow moved farther from a local thermodynamic equilibrium state. Future work could investigate optimal constraints to use for a mixture that is far from a local thermodynamic equilibrium state.

With the minor errors observed for the integrated RCCE simulations for both the nozzle and shock cases, these results suggest that one constraint can be used for simulations where both shocks and expansion occur (2D/3D flows). Once again, this relies on the assumption that small errors on individual species concentrations can be tolerated. Care should be taken when constructing a table for a complicated simulation, as the expected pressure, temperature, and ϕ range need to be considered before creating the table and running the simulation. In addition, if a more accurate description of the mixture composition is needed at all points in the flow, the effect of using more constraints to increase the accuracy of the RCCE method should be investigated. Finally, this section showed that for the two cases considered, the simple reconstructed ϕ profiles do a good job at predicting the performance of the corresponding fully integrated RCCE simulations.

X. Extension to the Martian Atmosphere

To evaluate whether these constraints can be extended to different systems, a gas mixture characteristic of the Martian atmosphere is tested using the same test problems previously described. A nine-species gas model is used, containing Ar, C, CO, CO_2, N, N_2, NO, O, and O_2. The previous five reactions used for the air system [Eqs. (21–25)] are still used, and in addition the following reactions are included:

$$O + CO \rightleftarrows CO_2 \tag{39}$$

$$O_2 + CO \rightleftarrows O + CO_2 \tag{40}$$

$$N + CO_2 \rightleftarrows NO + CO \tag{41}$$

$$C + O_2 \rightleftarrows O + CO \tag{42}$$

$$C + NO \rightleftarrows CO + N \tag{43}$$

These additional reactions and reactions rates are taken from GRI-Mech 3.0 [49]. An initial mixture composition of 96.00% CO_2,

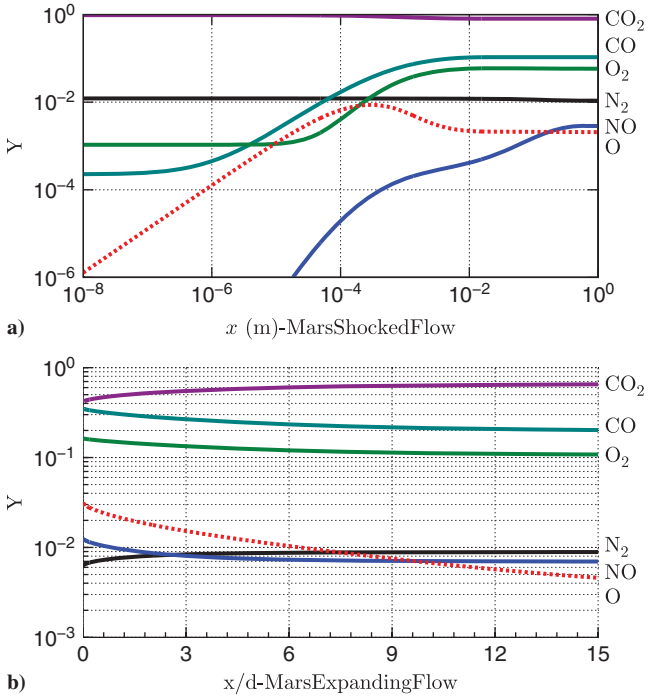

Fig. 13 Evolution of mass fractions for a gas mixture characteristic of the Martian atmosphere. a) 20 kPa and 297 K mixture processed by a 3 km/s ($M = 11.1$) normal shock. b) 4467 K and 45.2 MPa mixture undergoing a steady expansion.

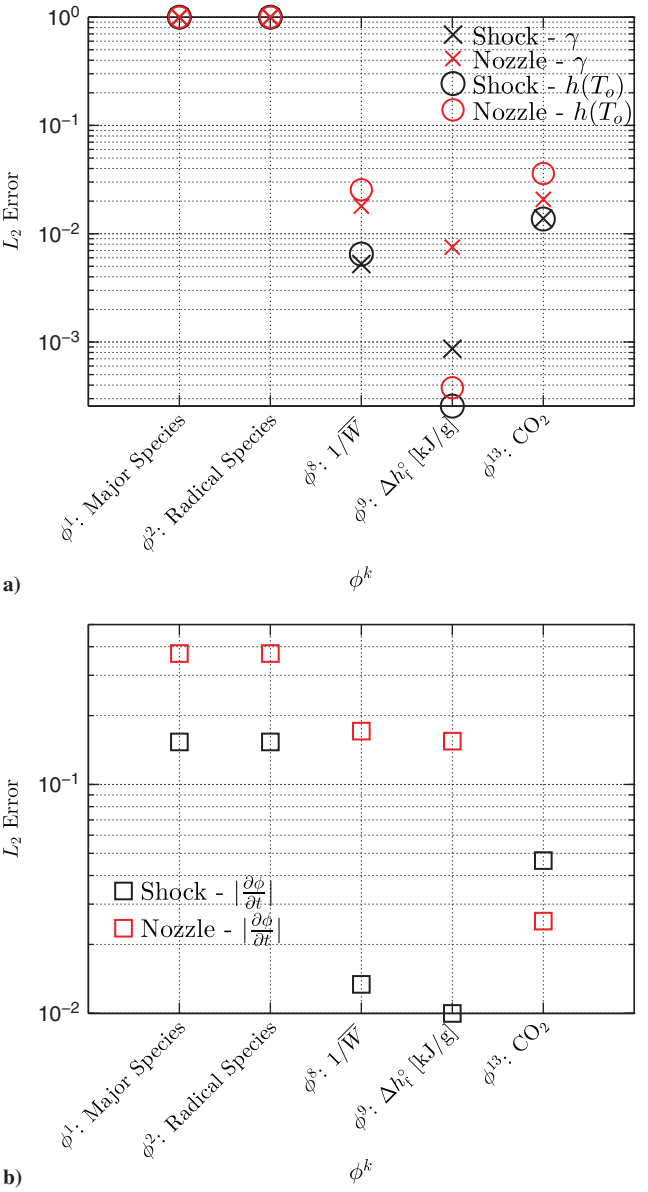

Fig. 14 L_2 error plot for a) $h(T_o)$ and γ, and b) $|\partial\phi/\partial t|$ for a Martian gas, calculated from Eq. (31). Each data set in a) is normalized by the maximum error from the respective test case. Calculated errors are individually normalized by $\max(|\partial\phi/\partial t|_{\text{Cantera}})$ in b). Different constraints are shown on the x axis (varying k), and their respective norms are plotted vertically.

1.93% Ar, 1.89% N_2, 0.14% O_2, and 0.04% CO (by volume) is used [50].

A similar analysis is performed as described in the previous sections for the air system, but only constraints consistent between the shock and nozzle conditions are compared for this new investigation. Figures 13a and 13b show the evolution of mass fractions through the shock test case and the nozzle test case, respectively. The same initial conditions are used in the shock gas as the previous air calculations (20 kPa and 297 K), but the postshock conditions are now different based on the properties of the new gas mixture.

Quantitative error calculations for the selected set of constraints, $k = 1, 2, 8, 9, 13$, are shown in Figs. 14a and 14b. The values for the C_i^k coefficients are altered from Table 3 to remain consistent with the new CO_2 mixture. $k = 13$ is chosen to represent a species constraint on CO_2, where $C^{13}_{i=CO_2} = 1$, and $C^{13}_{i\neq CO_2} = 0$. All of the C_i^k coefficients used in this section are the same between the shock and nozzle cases, for a given k. It is not surprising to note that CO_2 performs well as an individual species constraint, due to the large concentration of CO_2 present in the flow. The enthalpy of formation constraint performs the best overall once again, except when considering the error on $|\partial\phi/\partial t|$ for the nozzle case. The enthalpy of formation constraint is no longer a weighted sum of just the radical mass fractions, as nonradical species may have nonzero enthalpies of formation (e.g., CO). This constraint will be used for the simulations discussed in this section.

A fully integrated RCCE simulation is performed for the shock and nozzle test cases using the method outlined in Sec. IX. A table is constructed for this simulation with 100 points for pressure, temperature, and ϕ, respectively. The minimum and maximum values chosen are 100 kPa and 45.3 MPa, 2600 and 4800 K, and −8.7 and −4.5 kJ/g, for pressure, temperature, and ϕ, respectively, in order to cover the range of values expected for the two test cases. A tri-linear interpolation method is again used to interpolate values within the table. Figure 15a shows a comparison for the evolution of mass fractions, and Fig. 15b shows a comparison of the constraint evolution, for the shock test case. Similar to the air test case, some errors are made on the mass fractions directly behind the shock, and the solutions agree better farther downstream of the shock. A small difference in the final value of ϕ (∼0.03 kJ/g) is seen in Fig. 15b. This difference is once again caused by minor deviations between the solutions behind the shock. The differences in mass fractions between the final solution reached by the RCCE method and the detailed chemistry method are small, with the largest error in mass fraction observed between the two solutions being ∼0.004 for Y_{CO_2} at $x = 1$ m. Minor discrepancies are also seen in the final temperature and pressure states, with the error being ∼10 K and ∼20 Pa, for temperature and pressure, respectively. Figure 16a shows a comparison for the evolution of mass fractions, and Fig. 16b shows a comparison of the constraint evolution for the nozzle test case. Mass fractions of CO_2, CO, and O_2 are reproduced well, and minor errors are made on N_2, NO, and O. At $x/d = 15$, errors of ∼78 K, ∼3687 Pa, and ∼0.06kJ/g are made on temperature, pressure, and ϕ, respectively, between the two simulations. The largest discrepancy in mass fractions at $x/d = 15$ is found to occur on Y_{NO}, with a difference of ∼0.02.

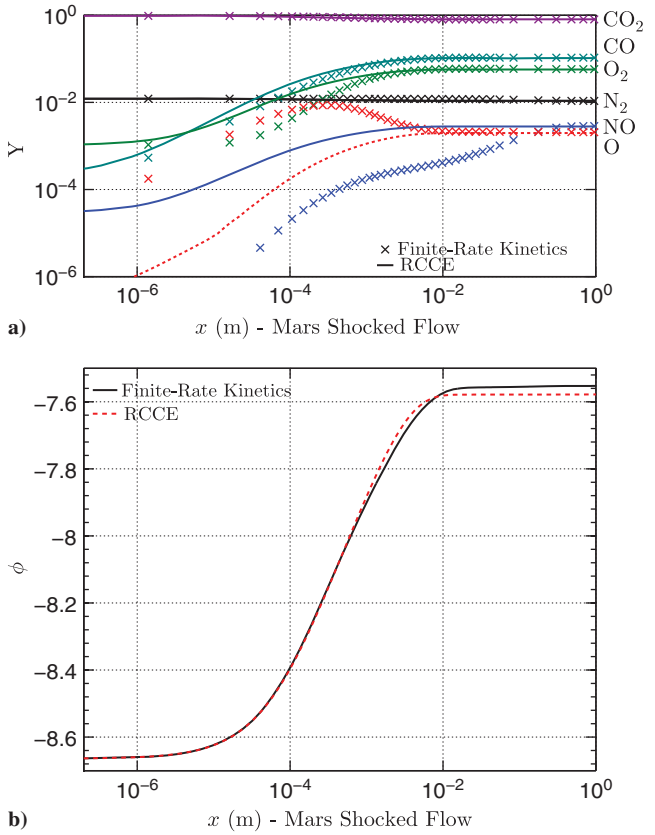

Fig. 15 Results for a fully integrated simulation using the RCCE method for the shock test case with a composition characteristic of the Martian atmosphere, constraining on enthalpy of formation. a) Mass fraction evolution; b) evolution of the constraint.

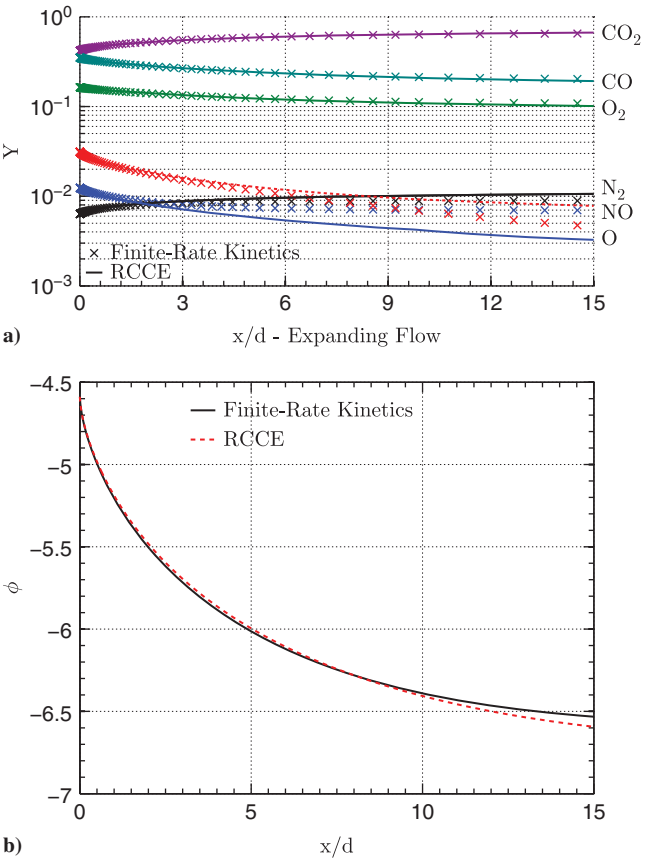

Fig. 16 Results for a fully integrated simulation using the RCCE method for the nozzle test case with a composition characteristic of the Martian atmosphere, constraining on enthalpy of formation. a) Mass fraction evolution; b) evolution of the constraint.

XI. Discussion

This work applied the RCCE method to compressible reacting flows that do not contain species that can easily be classified as reactants and/or products. In addition, predictions were made for constraint performance based on detailed chemical simulations that did not require a full RCCE simulation to be run. Both mixtures considered in this paper involve fairly simple reaction mechanisms (5 species and 5 reactions for air, and 9 species and 10 reactions for Mars). These reaction mechanisms have already been reduced; some chemical species were not included (such as NO_2, N_2O, NCO, and CN), and only the major reactions were considered. Nevertheless, the ability to use one constraint has reduced the number of equations that must be solved for these problems. With detailed, finite-rate chemistry, 5 species transport equations need to be solved in addition to the flow variables (T, P, w in 1D) for a total of 8 equations for air, and 13 equations for the Martian atmosphere. The number of equations solved is reduced for the fully integrated RCCE simulations, where only four equations need be solved simultaneously, regardless of the mixture considered.

The stiffness of the system of equations for the fully integrated RCCE simulations has also been reduced. This is illustrated with a simple timescale estimation. The simulation shown in Fig. 12a is considered at a point of $x/d = 2$. This location is chosen such that recombination reactions are still occurring in the nozzle, and the flow has had a finite amount of time to expand and depart from the thermodynamic equilibrium solution. At $x/d = 2$, the characteristic times associated with chemical reactions are $t_1^* \approx 5 \cdot 10^{-9}$ s, $t_2^* \approx 5 \cdot 10^{-7}$ s, and $t_3^* \approx 1.3 \cdot 10^{-6}$ s (Fig. 4b). At the same point, the timescale associated with the flow itself is $t_{\text{flow}}^* \approx 1.5 \cdot 10^{-5}$ s (Sec. VII.D). A timescale for the evolution of ϕ can be estimated from $t_\phi^* \approx (\Delta\phi/\partial\phi/\partial t)$, where $\Delta\phi$ is the change in ϕ throughout the entire nozzle. At $x/d = 2$, $t_\phi^* \approx 5.4 \cdot 10^{-5}$ s. The timescale associated with the rate of change of ϕ is now of the same order as that of the relevant fluid mechanical timescales. This result is characteristic of the RCCE method in general, and is not unique to this work.

Instead of having to perform constrained equilibrium calculations during a simulation, this work implemented RCCE methodology based on a tabulated approach. A single table can be created *once* before running simulations, and the same table used for multiple simulations. This was shown by using one table for both the shock and nozzle test cases for air, and one table for both the shock and nozzle Mars atmosphere test cases.

In general, the RCCE method can reduce the computational cost of a simulation both by reducing the number of equations that need to be solved and by decreasing the number of iterations required by reducing the stiffness of the equations being solved. Recent works have focused on the computational time that is saved when an optimized RCCE solver is used with more than one constraint [17,18]. The current work has focused on finding a single constraint that works well for flows that involve both shocks and steady expansions, where products and reactants cannot easily be identified. Because of the physical differences between these two kinds of flows, different chemical reactions are close to being in a local equilibrium for each flow, and so constraints based on reaction timescale analysis are difficult to implement. Future work should focus on extending the tabulated RCCE approach to more complicated gas models with more than one constraint so that a better understanding of the reduction of computational time associated with this specific implementation can be gained.

As was mentioned previously, there are limitations associated with the RCCE method. Some errors were made predicting species concentrations for all of the cases considered. For all test cases, it was observed that errors seen in the RCCE simulations can largely be attributed to the difficulties in reconstructing the composition of a mixture far from thermodynamic equilibrium using a constrained thermodynamic equilibrium calculation. If necessary, one way to

reduce these errors is to use more than one constraint to describe a system. This increases the computational complexity of the problem, but as more constraints are used, the solution from the RCCE method will tend toward the solution obtained from detailed chemistry simulations. In addition, Hiremath and Pope [20] show that solving for the RCCE constraints using Eq. (15) can introduce errors into the calculated solution, as the traditional RCCE implementation (used in this work) is based on a projection of the chemical source term onto the represented subspace that does not account for the noninvariance of the constrained equilibrium manifold. It is possible that if a larger chemical mechanism is used, in order to maintain an acceptable level of accuracy, not only would the number of constraints used need to be increased, but a more sophisticated RCCE methodology, such as RCCE/TIFS [20], would have to be implemented as well.

A simple tabulation method was implemented in this work, with a tri-linear interpolation algorithm. No attempts were made to locally refine the tables or to use higher-order interpolation methods. More advanced tabulation methods have been used successfully in conjunction with the RCCE method, for example, "*in situ* adaptive tabulation-rate-controlled constrained equilibrium (ISAT-RCCE)" [27]. Solution mapping using polynomial approximation (PRISM) [51] is another example of a method where only the accessed thermochemical state space is computed during the simulation, and stored in a table for use again later, similar to ISAT. These methods are most likely overly complex for the simple gas models considered in this work, but for more complicated gas mixtures, these advanced tabulation methods could be beneficial.

XII. Conclusions

A fundamental investigation into the performance of different constraints for the RCCE method was performed for reacting supersonic flows. Simple gas mixtures were used (5-species air and 9-species Mars atmosphere), and the effectiveness of different constraints was isolated by comparisons with detailed chemistry results. Formal timescale analysis techniques were combined with RCCE in order to determine possible new constraints. However, due to subjectivity involved with the numerical implementation of these constraints, and an inconsistent performance across simulations that involved both shocks and expansions, a new constraint based on the enthalpy of formation was proposed. This constraint performed well for both the nozzle and shock cases, though small errors in mass fractions were seen. In addition, this constraint worked well for the air mixture considered and for a gas mixture consisting primarily of CO_2 (characteristic of the Martian atmosphere). A tabulated methodology was used to implement the full RCCE simulations performed, and good agreement was seen between the RCCE simulations using one constraint and the detailed chemistry results.

Acknowledgment

Funding for this work was provided by the U.S. Air Force Office of Scientific Research, Grant FA9550-12-1-0472.

References

[1] Hornung, H., "Experimental Hypervelocity Flow Simulation, Needs, Achievements and Limitations," *Proceedings of the 1st Pacific International Conference on Aerospace Science and Technology*, Taiwan, 1993. doi:10.1017/jfm.2015.489

[2] Anderson, J. D., *Hypersonic and High-Temperature Gas Dynamics*, 2nd ed., AIAA, Resont, VA, 2006, Chap. 10. doi:10.2514/4.861956

[3] Lu, T., and Law, C. K., "A Directed Relation Graph Method for Mechanism Reduction," *Proceedings of the Combustion Institute*, Vol. 30, No. 1, 2005, pp. 1333–1341. doi:10.1016/j.proci.2004.08.145

[4] Lu, T., and Law, C. K., "A Criterion Based on Computational Singular Perturbation for the Identification of Quasi Steady State Species: A Reduced Mechanism for Methane Oxidation with NO Chemistry," *Combustion and Flame*, Vol. 154, No. 4, 2008, pp. 761–774. doi:10.1016/j.combustflame.2008.04.025

[5] Lu, T., Law, C. K., Yoo, C. S., and Chen, J. H., "Dynamic Stiffness Removal for Direct Numerical Simulations," *Combustion and Flame*, Vol. 156, No. 8, 2009, pp. 1542–1551. doi:10.1016/j.combustflame.2009.02.013

[6] Menon, S. K., Boettcher, P. A., and Blanquart, G., "Enthalpy Based Approach to Capture Heat Transfer Effects in Premixed Combustion," *Combustion and Flame*, Vol. 160, No. 7, 2013, pp. 1242–1253. doi:10.1016/j.combustflame.2013.02.008

[7] Muller, J.-M., *Elementary Functions: Algorithms and Implementation*, 2nd ed., Birkhäuser, Boston, MA, 2005, Chap 4. doi:10.1007/b137928

[8] Pepiot-Desjardins, P., and Pitsch, H., "An Efficient Error-Propagation-Based Reduction Method for Large Chemical Kinetic Mechanisms," *Combustion and Flame*, Vol. 154, No. 12, 2008, pp. 67–81. doi:10.1016/j.combustflame.2007.10.020

[9] Peters, N., "Reducing Mechanisms," *Reduced Kinetic Mechanisms and Asymptotic Approximations for Methane-Air Flames*, edited by Smooke, M. D., Vol. 384, Lecture Notes in Physics, Springer, Berlin, 1991, pp. 48–67. doi:10.1007/BFb0035362

[10] Goussis, D., and Lam, S., "A Study of Homogeneous Methanol Oxidation Kinetics Using CSP," *Symposium (International) on Combustion*, Vol. 24, No. 1, 1992, pp. 113–120. doi:10.1016/S0082-0784(06)80018-4

[11] Maas, U., and Pope, S., "Implementation of Simplified Chemical Kinetics Based on Intrinsic Low-Dimensional Manifolds," *Symposium (International) on Combustion*, Vol. 24, No. 1, 1992, pp. 103–112. doi:10.1016/S0082-0784(06)80017-2

[12] Maas, U., and Pope, S., "Simplifying Chemical Kinetics: Intrinsic Low-Dimensional Manifolds in Composition Space," *Combustion and Flame*, Vol. 88, No. 34, 1992, pp. 239–264. doi:10.1016/0010-2180(92)90034-M

[13] Janbozorgi, M., Ugarte, S., Metghalchi, H., and Keck, J. C., "Combustion Modeling of Mono-Carbon Fuels Using the Rate-Controlled Constrained-Equilibrium Method," *Combustion and Flame*, Vol. 156, No. 10, 2009, pp. 1871–1885. doi:10.1016/j.combustflame.2009.05.013

[14] Keck, J. C., "Rate-Controlled Constrained-Equilibrium Theory of Chemical Reactions in Complex Systems," *Progress in Energy and Combustion Science*, Vol. 16, No. 2, 1990, pp. 125–154. doi:10.1016/0360-1285(90)90046-6

[15] Law, R., Metghalchi, M., and Keck, J. C., "Rate-Controlled Constrained Equilibrium Calculation of Ignition Delay Times in Hydrogen-Oxygen Mixtures," *Symposium (International) on Combustion*, Vol. 22, No. 1, 1989, pp. 1705–1713. doi:10.1016/S0082-0784(89)80183-3

[16] Beretta, G. P., Keck, J. C., Janbozorgi, M., and Metghalchi, H., "The Rate-Controlled Constrained-Equilibrium Approach to Far-From-Local-Equilibrium Thermodynamics," *Entropy*, Vol. 14, No. 2, 2012, pp. 92–130. doi:10.3390/e14020092

[17] Hadi, F., and Sheikhi, M. R. H., "A Comparison of Constraint and Constraint Potential Forms of the Rate-Controlled Constraint-Equilibrium Method," *Journal of Energy Resources Technology*, Vol. 138, No. 2, 2015, Paper 022202. doi:10.1115/1.4031614

[18] Hadi, F., Janbozorgi, M., Sheikhi, M. R. H., and Metghalchi, H., "A Study of Interactions Between Mixing and Chemical Reaction Using the Rate-Controlled Constrained-Equilibrium Method," *Journal of Non-Equilibrium Thermodynamics*, Vol. 41, No. 4, Oct. 2016, pp. 257–278. doi:10.1515/jnet-2015-0052

[19] Hiremath, V., Ren, Z., and Pope, S. B., "A Greedy Algorithm for Species Selection in Dimension Reduction of Combustion Chemistry," *Combustion Theory and Modelling*, Vol. 14, No. 5, 2010, pp. 619–652. doi:10.1080/13647830.2010.499964

[20] Hiremath, V., and Pope, S. B., "A Study of the Rate-Controlled Constrained-Equilibrium Dimension Reduction Method and its Different Implementations," *Combustion Theory and Modelling*, Vol. 17, No. 2, 2013, pp. 260–293. doi:10.1080/13647830.2012.752109

[21] Janbozorgi, M., and Metghalchi, H., "Rate-Controlled Constrained-Equilibrium Theory Applied to the Expansion of Combustion Products in the Power Stroke of an Internal Combustion Engine," *International Journal of Thermodynamics*, Vol. 12, No. 1, 2009, pp. 44–50.

[22] Keck, J. C., and Gillespie, D., "Rate-Controlled Partial-Equilibrium Method for Treating Reacting Gas Mixtures," *Combustion and Flame*, Vol. 17, No. 2, 1971, pp. 237–241. doi:10.1016/S0010-2180(71)80166-9

[23] Lapointe, S., Bobbitt, B., and Blanquart, G., "Impact of Chemistry Models on Flame-Vortex Interaction," *Proceedings of the Combustion Institute*, Vol. 35, No. 1, 2015, pp. 1033–1040. doi:10.1016/j.proci.2014.06.091

[24] Nicolas, G., Janbozorgi, M., and Metghalchi, H., "Constrained-Equilibrium Modeling of Methane Oxidation in Air," *Journal of Energy Resources Technology*, Vol. 136, No. 3, 2014, pp. 032205-1–032205-7. doi:10.1115/1.4027692

[25] Nicolas, G., and Metghalchi, H., "Comparison Between RCCE and Shock Tube Ignition Delay Times at Low Temperatures," *Journal of Energy Resources Technology*, Vol. 137, No. 6, 2015, pp. 062203-1–062203-4. doi:10.1115/1.4030493

[26] Nicolas, G., and Metghalchi, H., "Development of the Rate-Controlled Constrained-Equilibrium Method for Modeling of Ethanol Combustion," *Journal of Energy Resources Technology*, Vol. 138, No. 2, 2015, pp. 022205-1–022205-11. doi:10.1115/1.4031511

[27] Tang, Q., and Pope, S. B., "Implementation of Combustion Chemistry by In Situ Adaptive Tabulation of Rate-Controlled Constrained Equilibrium Manifolds," *Proceedings of the Combustion Institute*, Vol. 29, No. 1, 2002, pp. 1411–1417. doi:10.1016/S1540-7489(02)80173-0

[28] Tang, Q., and Pope, S. B., "A More Accurate Projection in the Rate-Controlled Constrained-Equilibrium Method for Dimension Reduction of Combustion Chemistry," *Combustion Theory and Modelling*, Vol. 8, No. 2, 2004, pp. 255–279. doi:10.1088/1364-7830/8/2/004

[29] Ugarte, S., Gao, Y., and Metghalchi, H., "Application of the Maximum Entropy Principle in the Analysis of a Non-Equilibrium Chemically Reacting Mixture," *International Journal of Thermodynamics*, Vol. 8, No. 1, 2005, pp. 43–53.

[30] Yousefian, V., "A Rate-Controlled Constrained-Equilibrium Thermochemistry Algorithm for Complex Reacting Systems," *Combustion and Flame*, Vol. 115, Nos. 1–2, 1998, pp. 66–80. doi:10.1016/S0010-2180(97)00334-9

[31] Beretta, G. P., Janbozorgi, M., and Metghalchi, H., "Degree of Disequilibrium Analysis for Automatic Selection of Kinetic Constraints in the Rate-Controlled Constrained-Equilibrium Method," *Combustion and Flame*, Vol. 168, June 2016, pp. 342–364. doi:10.1016/j.combustflame.2016.02.005

[32] Janbozorgi, M., and Metghalchi, H., "Rate-Controlled Constrained-Equilibrium Modeling of H/O Reacting Nozzle Flow," *Journal of Propulsion and Power*, Vol. 28, No. 4, 2012, pp. 677–684. doi:10.2514/1.B34545

[33] Rabinovitch, J., and Blanquart, G., "A Computationally Efficient Approach to Hypersonic Reacting Flows," *29th International Symposium on Shock Waves 1: Volume 1*, Springer International Publ., Switzerland, 2015, pp. 173–178. doi:10.1007/978-3-319-16835-725

[34] Morr, A. R., and Heywood, J. B., "Partial Equilibrium Model for Predicting Concentration of CO in Combustion," *Acta Astronautica*, Vol. 1, No. 78, 1974, pp. 949–966. doi:10.1016/0094-5765(74)90062-9

[35] Kao, S., and Shepherd, J. E., "Numerical Solution Methods for Control Volume Explosions and ZND Detonation Structure," GALCIT FM2006-007, California Inst. of Technology, Pasadena, CA, 2006.

[36] Browne, S., Ziegler, J., and Shepherd, J. E., "Numerical Solution Methods for Shock and Detonation Jump Conditions," GALCIT FM2006-006, California Inst. of Technology, Pasadena, CA, 2006.

[37] Pope, S. B., "Gibbs Function Continuation for the Stable Computation of Chemical Equilibrium," *Combustion and Flame*, Vol. 139, No. 3, 2004, pp. 222–226. doi:10.1016/j.combustflame.2004.07.008

[38] Pope, S., "CEQ: A Fortran Library to Compute Equilibrium Compositions Using Gibbs Function Continuation," 2003, http://eccentric.mae.cornell.edu/pope/CEQ [retrieved June 2014]

[39] Pope, S., "The Computation of Constrained and Unconstrained Equilibrium Compositions of Ideal Gas Mixtures Using Gibbs Function Continuation," Cornell Univ. Rept. FDA 03-02, Ithaca, NY, 2003.

[40] Gou, X., Sun, W., Chen, Z., and Ju, Y., "A Dynamic Multi-Timescale Method for Combustion Modeling with Detailed and Reduced Chemical Kinetic Mechanisms," *Combustion and Flame*, Vol. 157, No. 6, 2010, pp. 1111–1121. doi:10.1016/j.combustflame.2010.02.020

[41] Goodwin, D. G., "An Open-Source, Extensible Software Suite for CVD Process Simulation," *Proceedings of Electrochemical Society (ECS)*, Vol. 14, Electrochemical Soc., Pennington, NJ, 2003, pp. 2003–2008. doi:10.2514/1.J052389

[42] Gordon, S., and McBride, B. J., "Thermodynamic Data to 20000 K for Monatomic Gases," NASA TP-1999-208523, 1999.

[43] McBride, B. J., Zehe, M. J., and Gordon, S., "NASA Glenn Coefficients for Calculating Thermodynamic Properties of Individual Species," NASA TP-2002-211556, 2002.

[44] Gupta, R. N., Yos, J. M., Thompson, R. A., and Lee, K. P., "A Review of Reaction Rates and Thermodynamic and Transport Properties for an 11-Species Air Model for Chemical and Thermal Nonequilibrium Calculations to 30000 K," NASA RP-1232, 1990.

[45] Parziale, N. J., "Slender-Body Hypervelocity Boundary-Layer Instability," Ph.D. Dissertation, California Inst. of Technology, Pasadena, CA, 2013.

[46] Rabinovitch, J., "Advancing EDL Technologies for Future Space Missions: From Ground Testing Facilities to Ablative Heatshields," Ph.D. Dissertation, California Inst. of Technology, Pasadena, CA, 2014.

[47] Pope, S., "Computationally Efficient Implementation of Combustion Chemistry Using In Situ Adaptive Tabulation," *Combustion Theory and Modelling*, Vol. 1, No. 1, 1997, pp. 41–63. doi:10.1080/713665229

[48] Regele, J. D., Knudsen, E., Pitsch, H., and Blanquart, G., "A Two-Equation Model for Non-Unity Lewis Number Differential Diffusion in Lean Premixed Laminar Flames," *Combustion and Flame*, Vol. 160, No. 2, 2013, pp. 240–250. doi:10.1016/j.combustflame.2012.10.004

[49] Smith, G. P., Golden, D. M., Frenklach, M., Moriarty, N. W., Eiteneer, B., Goldenberg, M., Bowman, C. T., Hanson, R. K., Song, S., Gardiner, W. C., Lissianski, V. V., and Qin, Z., "GRI-Mech 3.0," 1999, http://www.me.berkeley.edu/gri_mech/ [retrieved 4 March 2014].

[50] Mahaffy, P. R., , Webster, C. R., Atreya, S. K., Franz, H., Wong, M., Conrad, P. G., Harpold, D., Jones, J. J., Leshin, L. A., and Manning, H. et al., "Abundance and Isotopic Composition of Gases in the Martian Atmosphere from the Curiosity Rover," *Science*, Vol. 341, No. 6143, 2013, pp. 263–266. doi:10.1126/science.1237966

[51] Tonse, S. R., Moriarty, N. W., Brown, N. J., and Frenklach, M., "PRISM: Piecewise Reusable Implementation of Solution Mapping. An Economical Strategy for Chemical Kinetics," *Israel Journal of Chemistry*, Vol. 39, No. 1, 1999, pp. 97–106. doi:10.1002/ijch.199900010

V. Raman
Associate Editor